Title

Clonal and Quantitative In Vivo Assessment of Hematopoietic Stem Cell Differentiation Reveals Strong Erythroid Potential of Multipotent Cells

Journal

Stem Cell Reports, 12(4)

ISSN

2213-6711

Authors

Boyer, Scott W
Rajendiran, Smrithi
Beaudin, Anna E
et al.

Publication Date

2019-04-01

DOI

10.1016/j.stemcr.2019.02.007

Peer reviewed

Clonal and quantitative *in vivo* assessment of hematopoietic stem cell differentiation reveals strong erythroid potential of multipotent cells

Scott W. Boyer[1], Smrithi Rajendiran[1], Anna E. Beaudin[1], Stephanie Smith-Berdan, Praveen K. Muthuswamy, Jessica Perez-Cunningham, Eric W. Martin, Christa Cheung, Herman Tsang, Mark Landon, E. Camilla Forsberg*

Institute for the Biology of Stem Cells, Department of Biomolecular Engineering, University of California Santa Cruz, Santa Cruz, California 95064, USA

[1]Equal contribution

*Corresponding author: cforsber@ucsc.edu

SUMMARY

Hematopoiesis is arguably one of the best understood stem cell systems, however, significant challenges remain to reach a consensus understanding of the lineage potential, heterogeneity, and relationships of hematopoietic stem and progenitor cell populations. To gain new insights, we performed quantitative analyses of mature cell production from hematopoietic stem cells (HSCs) and multiple hematopoietic progenitor populations. Assessment of the absolute numbers of mature cell types produced by each progenitor cell revealed a striking erythroid dominance of all myeloid-competent progenitors assessed, accompanied by strong platelet reconstitution. All populations with myeloid potential also produced robust numbers of red blood cells and platelets *in vivo*. Clonal analysis by single cell transplantation and by spleen colony assays revealed that a significant fraction of HSCs and multipotent progenitors have multilineage potential at the single-cell level. These insights prompt an erythroid-focused model of hematopoietic differentiation.

INTRODUCTION

Hematopoietic stem cells (HSCs) differentiate via multiple, progressively committed progenitor cell populations to maintain a balanced number of mature blood cells. Despite extensive investigation, the lineage potential, heterogeneity and relationships of hematopoietic stem and progenitor cells (HSPCs) are under intense debate. Data from both single-cell transplantation and barcoding analysis support the existence of long-term, multi-lineage reconstituting clonal HSCs (Dykstra et al., 2007; Gerrits et al., 2010; Lu et al., 2011; Osawa et al., 1996; Yamamoto et al., 2013, 2018). However, differential lineage contribution from single cells suggests heterogeneity even within strictly defined HSC compartments (Benz et al., 2012; Yamamoto et al., 2013). Similarly, the heterogeneity and physiological roles of hematopoietic progenitor cells is hotly debated. Evidence from multiple studies indicate that FLK2-positive multipotent progenitors (MPP^F) serve as a developmental intermediate for all hematopoietic lineages, prior to the generation of progenitors restricted to either myeloid (common myeloid progenitors, CMPs) or lymphoid (common lymphoid progenitors, CLPs) fates (**Figure S1A**)(Akashi et al., 2000; Beaudin et al., 2014; Boyer et al., 2011, 2012; Forsberg et al., 2006; Kondo et al., 1997; Schlenner et al., 2010). While the existence of multipotent HSCs is widely accepted and recent *in situ* evidence support the existence of multilineage progenitor cells (Boyer et al., 2011; Busch et al., 2015; Sun et al., 2014), the degree of lineage commitment of hematopoietic populations remains controversial.

Several factors have made it difficult to assess the level of lineage commitment and lineage bias within hematopoietic subtypes. Tracking of mature RBC and Plt production from hematopoietic progenitor subsets *in vivo* was developed relatively recently; therefore the full spectrum of mature cell types is rarely simultaneously assessed. Substitute assays, such as hematopoietic differentiation *in vitro,* do not always accurately reflect differentiation *in situ* or upon transplantation *in vivo* (Boyer et al., 2012; Richie Ehrlich et al., 2011; Schlenner et al.,

2010). In addition, mature cell output from transplanted hematopoietic subtypes is seldom measured quantitatively, precluding accurate comparison of lineage output from specific hematopoietic subsets. Here, we use side-by-side absolute quantification of mature cell production and single cell *in vivo* assays to address the lineage contribution and functional heterogeneity of HSPCs. These insights were combined with previous data into a model of hematopoietic differentiation that reconciles multiple longstanding controversies in HSC biology.

RESULTS

Lineage potential of hematopoietic cell populations by traditional donor chimerism

To qualitatively and quantitatively assess the differentiation potential of distinct HSPC populations (**Figure S1A,B**), we performed comprehensive analyses of mature cell production upon transplantation into sublethally irradiated mice. UBC-GFP mice allowed for the simultaneous detection of donor-derived red blood cells (RBCs), platelets (Plts), granulocytes/myelomonocytes (GMs), B and T cells (**Figure S1C**). To enable detection of rare and transiently generated cell types, the peripheral blood (PB) of recipient mice was monitored at frequent and early time points post-transplantation.

We first displayed reconstitution as donor chimerism (donor-derived cells relative to host cells), as is commonly done (**Figure 1A-G, S1D**). Aside from a few notable exceptions and the addition of RBC analysis, our results largely agreed with previous reports (Akashi et al., 2000; D'Amico and Wu, 2003; Forsberg et al., 2006; Oguro et al., 2013; Yamamoto et al., 2013). Thus, HSCs gave rise to all five lineages analyzed, without evidence of decline for the duration of the experiments (16 weeks) (**Figure 1A**). MPP^F also gave rise to all five lineages analyzed, with clear declines in chimerism after 21-51 days posttransplantation (**Figure 1B, S1D**). Interestingly, although the Plt contribution from MPP^F was lower than GM, B, or T chimerism, as reported previously (Forsberg et al., 2006; Lai and Kondo, 2006), the RBC chimerism was similar to that of nucleated white blood cells. Both $FLK2^-$ and FLK2+ CMPs produced detectable levels of RBCs, Plts and GM, but not B and T, cells in the PB (**Figure 1C,D; S1D**). GMPs, MEPs and CLP^F contributed primarily to GM, RBC, and B cells, respectively (**Figure 1E-G; S1D**). Overall, these results agree with the lineage potential previously attributed to each of the HSPC populations.

Quantifying absolute numbers of mature cells produced by distinct progenitor populations

Reconstitution displayed as chimerism depends on both donor cell production and on the number of mature host cells present. To compare the effect of radiation conditioning on different types of host cells, we measured mature cell numbers at several time points post-sublethal irradiation. This analysis uncovered a dramatically cell type-specific variation in both the magnitude and kinetics of host cell decrease and recovery, with a rapid, greater than 1000-fold decrease in B cell numbers and only a ~1.4-fold, slower decrease in RBC numbers (**Figure 1H**). These host cell variations affect the perceived cell generation from transplanted cells when reconstitution is displayed as donor-to-host chimerism. To remove the host variable, we determined the absolute number of each donor-derived mature cell type in the PB after transplantation of different progenitor populations, displayed as the number of donor-derived cells per microliter of PB (**Figure 1M-S**). Even though these data were derived from the same transplantation experiments as for **Figure 1A-G**, the absolute quantification conveyed a remarkably different perspective on the ability of different progenitors to reconstitute hematopoiesis (compare **Figure 1A-G** with **1M-S**): with the exception of CLPs, RBC production exceeded all other cell types by orders of magnitude from all transplanted progenitor populations.

To determine whether this RBC dominance was only apparent in the blood, we accounted for differential tissue distribution of each cell type to convey the total number of cells produced per transplanted HSPC in the entire body of the recipient. Assessments of mature cell numbers and tissue distribution between major hematopoietic organs revealed that, as expected, RBCs far outnumbered the other cell types in PB (**Figure 1I**) and that the vast majority of the total RBCs present in a mouse were located in the PB (**Figure 1J**). Plts had a similar distribution pattern, whereas most GM cells were found in the BM. B cells distributed (in order of abundance) between BM, spleen, lymph nodes, and PB, and T cells between lymph

nodes, spleen, thymus, BM, and PB. Conversely, displaying each tissue based on the abundance of cell types revealed that blood is composed almost entirely of RBCs (87%) and Plts (12%) and that CD3+ T cells make up 78% of the hematopoietic cells in the thymus, whereas other tissues were less dominated by one cell type (**Figure 1K**). Combining the tissue distribution with PB cell counts provided an estimate of the total numbers of each cell type in a mouse (**Figure 1L**) that are consistent with previous reports (Kakumitsu et al., 2005; Nemzek et al., 2001).

These data enabled us to use the PB data (**Figure 1M-S**) to assess the absolute number of each mature cell type generated by each transplanted cell population in each recipient mouse (**Figure S2A-G**). While the magnitude of the difference between cells that mainly distribute to the blood (RBCs and Plts) and cell types that are dispersed between other tissues (GM, B and T cells) decreased when whole-body distribution was taken into account, the relative order of cell types produced was not altered (compare **Figure 1M-S** with **S2A-G**; except for GMPs, see below). Using modified Markov birth-death modeling and published mature cell half-lives, we tested the impact of cell half-life (ranging from ~1 day for GMs to ~150 days for T cells) on population size. Because the identity and half-lives of each intermediate population is not known, we modeled an "extreme half-life scenario" where the published half-lives for each mature population was used for all progenitor intermediates giving rise to that cell type to estimate the largest possible impact of the differential half-lives (**Figure S3A-B**). We then calculated a "birth rate" to distinguish *cell generation* (new cells produced; **Table S1** and **Figure S2A'G'**) from *cell accumulation* (number of cells present; **Table 1**). Over time, the differential half-lives have a significant impact; thus, our estimation of cell production by HSCs is different in the short-term (**Table 1, S2**) and long-term (**Table S1, S2**). Importantly, because repopulation from progenitor cells is transient, half-lives have less impact on estimation of mature cell production by progenitor cells, especially during the early time-points after transplantation that

we used for cell quantification (compare **Table 1** to **S1** and solid and dashed lines in **Figure S2A'-G'**; see **Figure 2A'-G'** for cell numbers and post-transplantation timepoints).

The absolute quantification revealed that RBCs were by far the most abundant cell type produced by each progenitor (**Figure 1M-S, S2A-G and Table 1**). The only exception were CLP^F, which stayed true to their reported lymphoid commitment by only producing B and T cells (**Figure 1S**) (Forsberg et al., 2006; Kondo et al., 1997; Schlenner et al., 2010). Of note, T cell production by CLP^F was more readily detectable when displayed as absolute numbers (**Figure 1S and S2G**) than as chimerism (**Figure 1G**). After RBCs, Plts were the next most abundant mature cell type produced. Despite the low Plt chimerism after transplantation of MPP^F, CMPs, CMP^F, MEPs, and GMPs (**Figure 1B-F**), donor-derived Plts outnumbered or equaled the GM, B, and T cells produced from each population (**Figure 1N-R, S2B-F, Table 1**). Surprisingly, GMPs, previously considered committed to myelomonocytic cell production (Akashi et al., 2000; Forsberg et al., 2006; Na Nakorn et al., 2002), produced more RBCs than GM cells and also contributed to Plts (**Figure 1Q, S2E, S4G-H, Table 1**). HSCs, CMPs and MEPs displayed a more expected reconstitution pattern. Notably, CMP^F gave rise to far greater numbers of RBCs than GM cells, with Plt production roughly equaling that of GM generation (**Figure 1P, S2D, Table 1**). Similarly, though MPP^F displayed complete multipotency, they produced RBCs and Plts in much greater abundance than they produced nucleated mature cells (**Figure 1N, S2B, Table 1**), defying reports that FLK2 expression signifies loss of MegE potential. Overall, the proportions of different mature cell types produced by all erythromyeloid-competent cells were strikingly similar (**Figure 1M-R, S2A-F, Table 1**).

Direct comparison of the mature cell production capacity of progenitor populations

To assess the relative reconstitution capacity of each progenitor cell type, we then compared the total output of each mature cell type per transplanted HSPC. Each HSC generated more of each mature cell type than any progenitor tested (**Figure 2A-E**). In addition, the time between

transplantation and the peak of mature cell production ("time-to-peak") was the longest for HSCs, and mature cells persisted without evidence of decline (**Figure 2A-E and 2A'-E'**). These properties are consistent with self-renewal and with HSCs existing at the top of the hematopoietic hierarchy (**Figure S1A**). Per transplanted cell, MPP^F gave rise to more RBCs, Plts, GMs, B-cells, and T-cells than any lineage-restricted progenitor (**Figure 2A-E**). In addition, the time-to-peak for mature cell production from transplanted MPP^F was shorter than for HSCs, but longer compared to lineage-restricted progenitors (**Figure 2A-E, 2A'-E'**). Likewise, the timing and total cell production from both CMP populations were in between the MPP^F and MEP. Relative to CMP^F, CMPs displayed more robust RBC and Plt generation (**Figure 2A-B; A'-B'**), while CMP^F excelled in GM production (**Figure 2C and C'**). While the capacity of CMP^F to produce RBCs and Plts *in vivo* contrasts with *in vitro* data where MegE output from CMP^F was not observed (Nutt et al., 2005), our results are consistent with the relative lineage preferences from previously described *in vitro* data, with CMP^F exhibiting a relative preference for GM production compared to CMP (**Figure 2A'-C' and Table 1**). GMPs produced the same cell types as CMP and CMP^F, but in fewer numbers and with the shortest time-to-peak for any HSPC (**Figure 2A-E, A'-E'**). Overall, these data are consistent with the developmental relationship between HSPCs displayed in **Figure S1A**.

MPP^F give rise to myeloid progenitors in vivo

The lineage potential and absolute number of cells produced can provide insights to the relative hierarchy of cell populations, but not direct mother-daughter relationships. To directly determine if MPP^F can give rise to erythro- and erythromyeloid-restricted progenitors, and to assess the extent of expansion of various progenitor populations, we performed phenotypic, quantitative, and functional analysis of donor-derived cells shortly after transplantation (**Figure 3A**). Two days after transplantation of HSCs or MPP^F, the phenotype of the donor cells in the recipient BM remained similar to their respective phenotype prior to transplantation (**Figure 3B-C**). By

days 7 and 14, transplanted HSCs maintained the self-renewing HSC pool while also repopulating phenotypic MPPs, “classical” (**Figure 3D^{1}-D^{2}**) and “alternative” myeloid progenitors (**Figure 3E^{1}-E^{2}**), as well as EPs and mature GM cells (**Figure 3H^{1}-H^{2}**). Few HSC-derived B and T cells were detected within the 14-day analysis period. BM analyses at days 4, 7, 11 and 14 revealed that MPP^{F} repopulated all types of erythromyeloid progenitors and mature cells (**Figure 3F^{1}-I^{4}**). Quantification of the absolute donor-derived cell numbers showed substantial expansion of donor-derived cells during the analysis period (**Figure 3D$^{1\text{-}2\text{‘}}$-I$^{1\text{-}4\text{’}}$ and S4A-D**). By day 14, the transplanted HSCs had given rise to ~2 million and MPP^{F} to nearly 4 million myeloid progenitor cells (**Figures 3D$^{1\text{-}2\text{‘}}$-G$^{1\text{-}4\text{’}}$**). While MPP^{F} clearly produced more B cells compared to HSCs within this timeframe (**Figure 3H$^{1\text{‘}}$-I$^{4\text{’}}$**), the proportion of progenitor cells generated by HSCs and MPP^{F} were similar (**Figure 3D$^{1\text{‘}}$-I$^{4\text{’}}$**). For example, comparing CMP/GMP/MEP proportions from HSCs at D14 with CMP/GMP/MEP from MPP^{F} at D11 revealed that distributions were not statistically significantly different (**Figure 3D$^{1\text{-}2\text{’}}$** versus **3F$^{1\text{-}4\text{’}}$**). Indeed, GMPs were the second most abundantly produced progenitor population from both HSCs (~1.3M GMPs by day 14) and MPP^{F} (~2.2M GMPs; approximately 2-fold more than from HSCs), after EPs (~13M from HSCs and, as with GMP generation, ~2-fold more (~26M) EPs from MPP^{F}). Interestingly, these experiments did not reveal a clear hierarchy between CMPs and their presumed GMP and MEP descendants, as GMPs outnumbered CMPs at all timepoints from both HSCs and MPP^{F}. Secondary transplantation of HSC- and MPP^{F}-derived CMPs, GMPs, MEPs, and EPs confirmed that these populations have the same lineage potential as the corresponding cell population in primary transplantation (**Figure S4E-L**). MPP^{F} were also capable of producing phenotypic CLPs, although in significantly lower numbers compared to erythromyeloid-restricted progenitors (~35-fold and ~220-fold differences at Days 7 and 14, respectively; **Figure S4M-N**). Quantitatively, these experiments demonstrate that there is substantial expansion in progenitor cell numbers in the BM soon after transplantation, that HSCs and MPP^{F} produce various erythromyeloid progenitors in roughly the same proportions,

and that MPP^F produce more erythromyeloid- than lymphoid-restricted progenitor cells. Qualitatively, these data provide direct evidence that transplanted MPP^F produce all types of erythromyeloid- and lymphoid-competent progenitor cells, consistent with full multipotency.

Transplantation of single MPP^F provides multilineage reconstitution

It is clear from the data presented in **Figures 1M-N, 3F-I, S2A-B** that transplantation of multiple MPP^F results in a similar cell production profile as HSCs. However, population data cannot determine if the MPP^F compartment is functionally homogeneous with each cell being multipotent (**Figure 4A**, Multipotency model (Boyer et al., 2012)), if MPP^F are a heterogeneous population of committed progenitors that share a common phenotype (**Figure 4A**, Commitment model), or a combination of the two. To differentiate between these possibilities, we implemented two *in vivo* clonal approaches: single-cell transplantation and analysis of single-cell derived CFU-S.

Single-cell transplantation of one HSC or one MPP^F led to detectable levels of donor-derived cells in 19% and 17% of mice, respectively (**Figure 4B; S5**). Eight out of the 20 reconstituted recipients of a single HSC had donor-derived cells of all 5 lineages investigated (**Figure 4C; S5**). This may be an underestimate of their true capacity, as some quiescent HSCs do not produce progeny until many weeks after transplantation or until secondary transfer (Yamamoto et al., 2013). 55% of mice reconstituted with a single HSC produced cells of at least one myeloid lineage (RBCs, Plts, and/or GMs) and one lymphoid lineage (B-cells and/or T-cells) and were therefore categorized as multipotent (**Figure 4B and C**). The remaining positive recipients of single HSCs produced only myeloid cells, whereas none produced only lymphoid cells (**Figure 4B and C**). None of the single MPP^F gave rise to all five cell types analyzed. Importantly, however, some single MPP^F gave rise to four different types of mature cells, and a considerable fraction of single MPP^F (43%; 9/21) generated both myeloid and lymphoid cells (**Figure 4B and D**). Increasing the number of transplanted MPP^F to 5 or 25 cells led to a higher

frequency of recipients with detectable donor cells (**Figure 4B**), an increased number of cell types detected (**Figure 4D-F**), and an increase in donor chimerism levels (**Figure 4H-J**; average overall reconstitution from 1, 5 and 25 MPP^F was 0.9%, 1.5% and 2.2%, respectively). 25 MPP^F were sufficient for combined myeloid and lymphoid detection in 100% of recipients, whereas mice transplanted with 5 or 1 MPP^F or a single HSC were multilineage reconstituted at lower frequencies (37.5%, 43%, and 55%, respectively; **Figure 4B-F**). Although a single MPP^F did not contribute as robustly to recipient chimerism as a single HSC (**Figure 4G-H**; average overall reconstitution levels were 0.9% and 8%, respectively), more RBCs than any other mature cell type were generated from both HSCs and MPP^F (**Figure 4K-N**).

Despite high frequency of combined myeloid and lymphoid reconstitution by MPP^F, we noted that MPP^F led to only GM, only B and/or combined GM/B cell reconstitution of some recipients, whereas HSCs did not. In addition, some myelo/lympho reconstitution occurred in unexpected combinations, such as only RBCs and B cells (mouse #6 for single MPP^F, mouse #9 for 25 MPP^F, and mice #s 8 and 9 for 5 MPP^F). GM and B cells occurred together in several mice, without detection of T cells. Indeed, T-cell readout was the most difficult lineage to detect from both HSC and MPP^F transplants (**Figure 4C-F**). As different mature cell types in the host are depleted to different extents upon sublethal (**Figure 1H**) and lethal (**Figure 4O**) irradiation, and donor-derived progeny are produced with different kinetics from different HSCs and MPP^F (**Figure 2A'-E'**), we hypothesized that the kinetics of host and donor cells differentially affects donor-derived cell detection. Superimposing the decline and recovery of host cells with the production of mature cells by HSCs or MPP^F revealed that RBC production from both HSCs and MPP^F largely coincide with the reduction in host RBCs (**Figure 4P**), facilitating detection of donor-derived RBCs in recipient mice. In contrast, neither HSCs nor MPP^F produce large numbers of T cells until after host T cell numbers have significantly recovered (**Figure 4T**), contributing to poor detection of T cells in mice transplanted with a single cell (**Figure 4C and D**). Similarly, the timing of GM and B cell production from MPP^F occur near the low point of host

GM and B cells, whereas the main contribution of HSCs to GM and B cells occur after host cell recovery (**Figure 4R and S**). The fact that B cells is the host cell type most affected by irradiation (**Figure 1H and 4O**) and that MPP^F produce B cells prior to host recovery whereas HSCs do not (**Figure 4S**) contribute to the relatively high frequency of B cell detection in mice transplanted by a single MPP^F, as well as the more apparent contribution of CLP^F to B cells than T cells (**Figure 1G and S, Figure S6**).

Multilineage reconstitution from single HSCs and MPP^F in spleen colony assays

To test the multipotency of clonal HSCs and MPP^F by an independent method, we analyzed donor-derived colony-forming units of the spleen (CFU-S). Like single-cell transplants, this assay measures clonal lineage potential, as each colony consists of progeny from a single cell (Becker et al., 1963; Weber et al., 2011). In support of the clonal origin of CFU-S, we observed only single-color colonies when a mixture of Tomato+ cells and GFP+ cells were transplanted into the same recipient (**Figure 5A**). To test for multilineage potential of single cells, we examined individually dissected CFU-S for erythroid progenitors (EPs), megakaryocytes (Megs), GMs, and B-cells (**Figure 5B**). It is highly improbable that CFU-S colonies were contaminated with circulating, donor-derived mature cells, as donor contribution within individual CFU-S was substantially higher than the donor cell chimerism in the peripheral blood (compare **Figure 5B** to **5C**). T-cell output was not assessed as T-cells require extended development in the thymus, and are not produced in the spleen or in the timeframe of this assay.

Of 13 HSC-derived CFU-S, 6 (46%) contained all four lineages that can be detected in this assay (EPs, Megs, GMs, and B-cells; **Figure 5D, red bar; Figure 5E**). The remaining colonies lacked B cells and were thus a mixture of myeloid lineages. Similarly, 6 of the 18 (33%) single-MPP^F-derived colonies contained all four lineages (**Figure 5D, E**). Other MPP^F-derived CFU-S contained various combinations of myeloid only and/or myeloid plus B cells. The proportion of myelo/lympho, myeloid only, or lymphoid only colonies produced by HSCs versus

MPP^{F} were not significantly different (**Figure 5E**). All colonies visible to the eye contained erythroid cells. In fact, the vast majority of total cells produced were erythroid cells (**Figure 5F**), and CFU-S derived from CMP, CMP^{F}, and MEP contained only EPs (**Figure 5D**). The absence of additional lineages from myeloid progenitors is likely due to their reduced total cell production compared to HSCs and MPP^{F} (**Figure 2A-C**), limiting our ability to detect mature cells that are not produced in as high abundance as erythrocytes. The CFU-S data, like the single cell transplantations, demonstrate that a substantial fraction of both HSCs and MPP^{F} are multipotent at the single cell level.

DISCUSSION

A quantitative perspective of progenitor repopulation capacity

By simply quantifying the absolute number of mature cells generated per transplanted stem and progenitor cell, we provide a different perspective of the regenerative capacity of HSCs and several progenitor populations. Our strategy revealed that all progenitor cells with myeloid potential produce far more RBCs than any other cell type (**Table 1 and Figure 1M-S, 2A-E, 2A'-E', 3A-F, 4K-N and 5D-F**). As illustrated by the concordance with previous findings when the same results were displayed as traditional donor chimerism (**Figure 1A-G**), our results are not due to differences in gating strategies, cell population purity, or transplantation methods. Rather, the insights were reached by eliminating the drastically variable fluctuations in host cell disappearance and recovery (**Figure 1H and 4O**) and by taking into account the absolute numbers of each mature cell type, including RBCs and Plts, produced by each stem and progenitor cell (**Figure 2A-E, 2A'-E', S2**). As transplanted donor cells differ not only in the types of cells generated, but also in the number, timing and duration of mature cell production, each progenitor cell has a distinct reconstitution pattern. In addition, the half-lives of mature cell types vary considerably. Collectively, these dynamics differentially affect the ability to detect and quantify the contribution of different donor populations to each mature lineage, as exemplified in **Figure 4P-T** and **S6**. Absolute quantification of donor-derived cells removes host variables and therefore facilitates comparative assessment of reconstitution both across lineages and between transplanted populations.

Unexpected lineage potential of hematopoietic progenitor populations

The lineage potential that we uncovered was in some cases unexpected. For example, GMPs have been reported to express few erythroid-associated genes and to lack MegE potential (Akashi et al., 2000; Forsberg et al., 2006; Paul et al., 2015; Pronk et al., 2007) and CMP^F produce few megakaryocyte/erythroid colonies *in vitro* (Nutt et al., 2005), whereas our

experiments here revealed that CMP^F and GMPs produce RBCs and Plts (**Figure 1D-E, 1P-Q, 2A-C, 2A'-C', 3A-J, S2, S4E-H, Table 1**). Significant heterogeneity of myeloid progenitor populations, especially classical CMPs, has been reported (Miyawaki et al., 2015; Paul et al., 2015; Perié et al., 2015), confounding interpretation of lineage potential. While the purity of bulk populations is not absolute, contamination cannot explain the differences between the lineage potential apparent in **Figure 1A-G** and **1M-S,** as these data are derived from the exact same experiments. Other possible contributors to the contradictory findings include differences between the in vitro and in vivo assay conditions, limits of detection, and the relatively recent development of mice that make it possible to directly track RBCs and Plts *in vivo*. The cell production capacity varies drastically between different progenitors: our estimates revealed that each MPP^F produces, on average, ~800,000 cells, whereas one GMP gives rise to ~47 progeny (43 RBCs, 1 Plt and 4 GM cells; **Figure 2A'-E'**). The low burst size of GMPs precludes detection of progeny in single cell transplants and in CFU-S; thus, the data presented here do not conclusively rule out that RBC and/or Plt generation from presumed GMPs is from "contaminating" cells. Notably, whereas we readily detected GFP+ RBCs and Plts in every recipient of GMPs in both primary and secondary transplantation experiments (**Figures 1E,Q and S4G,H**), we did not observe RBC or Plt production from CLPs (**Figure 1G and S**) or Plts from EPs (**Figure S4K-L**), indicating that the technical purity of our transplanted cell populations is good. In future studies we will test whether GMPs, like MPP^Fs, fit the "default" model proposed below by displaying significant in vivo MegE potential that is not readily detected in vitro. In contrast, the numbers of RBCs produced by CMP and CMP^F (averaging ~140,000 and 35,000, respectively) were sufficient for detection of EPs in CFU-S (**Figure 5D**), whereas detection of Plts from CMP, CMP^F, GMPs and MEPs required transplantation of higher numbers of progenitors. We previously demonstrated that Flk2+ MPPs give rise to all lineages, including erythroid cells, *in situ* at both steady-state and under stress, as well as upon transplantation (Boyer et al., 2011, 2012; Forsberg et al., 2006). Collectively, our results indicate that it is

difficult to separate functional RBC and Plt potential from GM potential in vivo, reinforcing the existence of functional CMPs and the retention of RBC capability across several phenotypically distinct populations.

CLP^F appear restricted to B and T cell generation

The only population in our study that did not produce RBCs and Plts was CLP^F. CLP^F also lacked detectable GM potential and therefore appear committed to the lymphoid fate, in agreement with their initial designation as CLPs (Kondo et al., 1997) and with *in vivo* lineage tracing experiments (Schlenner et al., 2010). Interestingly, while B cell production was readily detectable, T cell capacity was more apparent by absolute quantification than by donor chimerism data (compare **Figure 1G** to **1S**). The relative difficulty in detecting CLP^F-derived T cells can be attributed, in part, to host T cells being less affected by irradiation compared to host B cells (~20-fold versus ~1,000 fold, respectively; **Figure 1H**) and because host T cell numbers recover before CLP^F-derived T cells start accumulating (~day 19; **Figure 1S and S6**). In contrast, CLP^F-derived B cells are detected as early as Day 9 after transplantation, closely coinciding with the sharp reduction in host B cells (**Figure S6**). Their more limited lineage potential and lower expansion capacity is consistent with CLP^F residing hierarchically downstream of MPP^F. However, our calculations estimated that one MPP^F gives rise to equal numbers of B cells (~2,500) and T cells (~2,700), whereas one CLP^F gives rise to 10-fold more B cells than T cells (420 versus 42) (**Figure 2D'-E'**). This appears inconsistent with a direct and exclusive MPP^F-to-CLP^F transition, but rather evokes additional intermediate populations and/or flexibility in differentiation pathways from upstream progenitors.

Multilineage differentiation potential of single HSCs and MPP^F

It is clear from both the chimerism (**Figure 1B**) and absolute cell number data (**Figure 1N and 2A-E**), as well as previous publications (Forsberg et al., 2006; Miyawaki et al., 2015; Yamamoto

et al., 2013), that despite downregulation of erythroid-associated genes (Forsberg et al., 2006; Moignard et al., 2013), MPP^F are multipotent at the population level. Here, we also showed that a substantial fraction of MPP^F is multipotent at the single cell level. In CFU-S assays, MPP^F produced both myeloid and lymphoid cells in 67% of the colonies, with the remaining colonies consisting of myeloid cells only (**Figure 5D-E**). While the CFU-S frequency from MPP^F is lower than that from HSCs (~1/78 versus 1/33 (Beaudin et al., 2014; Forsberg et al., 2006)), CFU-S capability is clearly an underestimate of the MegE potential of a cell as far more than 1/33 HSCs are multipotent in other assays. Indeed, the CFU-S frequency increases ~10-fold when HSCs or MPP^F are injected directly into the spleen as opposed to IV (Beaudin et al., 2014). Collectively, these data demonstrate that the ability of MPP^F to generate MegE cells is substantially greater than estimated by CFU-S alone.

A similar proportion of HSCs and MPP^F displayed combined myelo/lymphoid potential at the clonal level upon single cell transplantation (55% of HSCs and 43% of MPP^F; **Figure 4B-C**). Our numbers are similar to those of Yamamoto et al, who found that 56% (9/16 mice) of "LMPPs" (in their report defined as KLS CD34+FLK2+, a population significantly overlapping with our MPP^F) displayed combined myelo/lymphoid readout (Yamamoto et al., 2013). *In vivo* evidence for the existence of clonal MPP was also provided by *in situ* barcoding studies (Rodriguez-Fraticelli et al., 2018; Sun et al., 2014). The exact proportion of uncommitted cells within the HSC and MPP^F compartment is difficult to estimate, as variable lineage outputs could be a result of detection limits (progeny were produced but not in sufficient numbers to detect), stochasticity (the transplanted cell happened to encounter a particular combination of cytokines), population heterogeneity (a proportion of the cells are multipotent, whereas some are not), or a combination of the three. Few studies have tested the full lineage potential of MPP^F, but the heterogeneity of HSCs has been tested and debated extensively (Ema et al., 2014; Hock, 2010; Kokkaliaris et al., 2016; Schroeder, 2010). The HSC results are highly relevant for the heterogeneity of MPP^F: a lineage restricted cell (a committed "HSC") cannot

give rise to a cell with greater lineage potential (a multipotent MPP). Thus, the proportion of multipotent cells within the MPP^F fraction must be equal to or smaller than the fraction of HSCs that are multipotent (**Figure 4A**; (Boyer et al., 2012)). Conversely, if some MPP^F are uncommitted, an equal or greater proportion of HSCs and other upstream populations should also be uncommitted. In our experiments, the frequency of single cells with combined myelo/lympho potential is similar for HSCs and MPP^F (55% and 43% for singly transplanted HSCs and MPP^F, respectively, and 46% and 67% for HSCs and MPP^F in CFU-S). Given that it is harder to detect progeny from MPP^F than from HSCs, the extent of lineage restriction upon the transition from HSCs to MPP^F appears quite low. Existence of fully multipotent progenitor cells is consistent with the notion that steady-state hematopoiesis is largely sustained by MPPs rather than HSCs (Busch et al., 2015; Sun et al., 2014).

RBC production as the default hematopoietic fate

Previous studies have shown that substantial amplification of RBC production occurs at the level of erythroid-committed progenitors and precursors. While the overall dominance of RBC production should not be unexpected, models of hematopoietic differentiation rarely take the vastly different numbers of mature cells into account. The fact that cell populations like MPP^F and GMPs, despite their poor ability to generate MegE cells in vitro and clear downregulation of erythroid-driving genes, generate RBCs not only in the largest absolute numbers, but also in roughly similar relative proportions as compared to other HSPCs, was particularly surprising. This discordance of gene expression and functional differentiation potential may hamper efforts to construct lineage maps based on transcriptome data. To reconcile these apparent discrepancies, we propose a model based on functional lineage potential where RBC production is the default pathway (**Figure 6**). In this model, MegE potential is gained upon specification of HSCs from a hematovascular precursor. HSCs, at all stages of development, thus have inherent capability to generate RBCs and Plts, but not necessarily GM, T and B cells. This notion makes

sense through ontogeny and as a mechanism to ensure survival, and fits with newly proposed views of human hematopoiesis (Notta et al., 2016). Our model proposes that differentiation into alternative fates is accomplished downstream of HSCs by the combination of two mechanisms: increased expression of proteins promoting GM, B, and/or T cell differentiation, and a concurrent decrease in expression of genes driving RBC and Plt generatoin. In vivo, continuous expression of MegE-promoting genes does not appear necessary for retention of RBC and Plt capability, conceivably because MegE differentiation has already been initiated. Unless exposed to sufficient concentrations of factors to alter this path, most hematopoietic progenitors will therefore produce primarily RBCs and Plts. Conversely, downregulation of MegE-promoting genes may be necessary for deviation from this default pathway to allow for the relatively rare production of GM, B and T cells. When the default pathway is interrupted (removal of cells from their natural environment), progenitors that have downregulated MegE-specifying receptors (MPP^F, CMP^F and GMPs) are unable to *reinitiate* MegE production. Thus, they perform relatively poorly in MegE assays *in vitro* (Adolfsson et al., 2005; Nutt et al., 2005; Pronk et al., 2007). As MPP^F, CMP^F and GMPs have acquired expression of receptors that promote GM or lymphoid fates, they are reactive to the corresponding cytokines and consequently readily differentiate *in vitro* into cell types that normally (*in vivo*) represent alternative fates. The proposed model impacts our understanding of erythroid-specific versus pan-hematopoietic disorders, and also provides explanations for the discordant lineage potential by *in vivo* and *in vitro* strategies and for the disconnection between gene expression patterns and functional cell production *in vivo*. Collectively, MPP^F may be viewed more accurately as cells that have *gained* GM, B and T potential than as cells that have *lost* MegE potential. This view is supported by our previous demonstration that all hematopoietic lineages are derived via a FLK2+ stage in situ and upon transplantation (Boyer et al., 2011, 2012); by FLK2 promoting expansion of all mature blood cell types (Beaudin et al., 2014); and by recent reports pointing to MPPs, rather than

HSCs, as the major source of mature hematopoietic cells during steady-state hematopoiesis *in situ* (Busch et al., 2015; Sun et al., 2014).

EXPERIMENTAL PROCEDURES

Transplantation assays

Hematopoietic cells were isolated from BM isolated from murine femurs and tibias from wild-type (C57Bl6) or UBC-GFP mice (Schaefer et al., 2001) in accordance with UCSC guidelines, as described in the supplemental methods and previously (Beaudin et al., 2014, 2016, Smith-Berdan et al., 2011, 2015; Ugarte et al., 2015).

Mature cell quantification

A known volume of peripheral blood was mixed with an antibody solution containing a known quantity of Calibrite-APC beads prior to flow cytometry analysis. For tissues, a known quantity of beads was added to each tissue preparation prior to antibody staining and analysis. The number of beads counted by flow cytometry was used to calculate the number of mature cells per microliter of blood or within each tissue. The distribution of mature hematopoietic cells in a mouse was measured in the blood obtained by perfusion; in bone marrow by analysis of two femurs and tibias; spleen; thymus; and lymph nodes (inguinal, axillary, and superficial cervical).

Single-cell transplants

Individual HSCs and MPP^F were double-sorted into separate wells on Terasaki plates using a FACSAriaIII from lineage-depleted bone marrow cells from UBC-GFP mice, similar to our previous reports (Byrne et al., 2017; Cole et al., 2018) and as detailed in the supplemental methods.

ACKNOWLEDGEMENTS

We thank Forsberg lab members for comments on the manuscript. This work was supported by an NIH/NHLBI award (R01HL115158) to ECF; by CIRM Training grant TG2-01157 to SWB and AEB; by NIH/NIGMS T32-GM008646 to SWB and JPC; by an HHMI Gilliam pre-doctoral award

to JPC; by CIRM SCILL grant TB1-01195 to EWM via San Jose State University; and by CIRM Shared Stem Cell Facilities (CL1-00506) and CIRM Major Facilities (FA1-00617-1) awards to UCSC.

REFERENCES

Adolfsson, J., Månsson, R., Buza-Vidas, N., Hultquist, A., Liuba, K., Jensen, C.T., Bryder, D., Yang, L., Borge, O.-J., Thoren, L.A.M., et al. (2005). Identification of Flt3+ Lympho-Myeloid Stem Cells Lacking Erythro-Megakaryocytic Potential. Cell *121*, 295–306.

Akashi, K., Traver, D., Miyamoto, T., and Weissman, I.L. (2000). A clonogenic common myeloid progenitor that gives rise to all myeloid lineages. Nature *404*, 193–197.

Beaudin, A.E., Boyer, S.W., and Forsberg, E.C. (2014). Flk2/Flt3 promotes both myeloid and lymphoid development by expanding non-self-renewing multipotent hematopoietic progenitor cells. Exp. Hematol. *42*, 218–229.e4.

Beaudin, A.E., Boyer, S.W., Perez-Cunningham, J., Hernandez, G.E., Derderian, S.C., Jujjavarapu, C., Aaserude, E., MacKenzie, T., and Forsberg, E.C. (2016). A Transient Developmental Hematopoietic Stem Cell Gives Rise to Innate-like B and T Cells. Cell Stem Cell *19*, 768–783.

Becker, A.J., McCulloch, E.A., and Till, J.E. (1963). Cytological demonstration of the clonal nature of spleen colonies derived from transplanted mouse marrow cells. Nature *197*, 452–454.

Benz, C., Copley, M.R., Kent, D.G., Wohrer, S., Cortes, A., Aghaeepour, N., Ma, E., Mader, H., Rowe, K., Day, C., et al. (2012). Hematopoietic stem cell subtypes expand differentially during development and display distinct lymphopoietic programs. Cell Stem Cell *10*, 273–283.

Boyer, S.W., Schroeder, A. V., Smith-Berdan, S., and Forsberg, E.C. (2011). All Hematopoietic Cells Develop from Hematopoietic Stem Cells through Flk2/Flt3-Positive Progenitor Cells. Cell Stem Cell *9*, 64–73.

Boyer, S.W., Beaudin, A.E., and Forsberg, E.C. (2012). Mapping differentiation pathways from hematopoietic stem cells using Flk2/Flt3 lineage tracing. Cell Cycle *11*, 3180–3188.

Busch, K., Klapproth, K., Barile, M., Flossdorf, M., Holland-Letz, T., Schlenner, S.M., Reth, M., Höfer, T., and Rodewald, H.-R. (2015). Fundamental properties of unperturbed haematopoiesis from stem cells in vivo. Nature *518*, 542–546.

Byrne A, Beaudin AE, Olsen HE, Jain M, Cole C, Palmer T, DuBois RM, Forsberg EC, Akeson M, Vollmers C. (2017) Nanopore long-read RNAseq reveals widespread transcriptional variation among the surface receptors of individual B cells. Nat Commun. *8*:16027.

Cole C, Byrne A, Beaudin AE, Forsberg EC, Vollmers C. (2018) Tn5Prime, a Tn5 based 5' capture method for single cell RNA-seq. Nucleic Acids Res. *46*,e62.

D'Amico, A., and Wu, L. (2003). The Early Progenitors of Mouse Dendritic Cells and Plasmacytoid Predendritic Cells Are within the Bone Marrow Hemopoietic Precursors Expressing Flt3. J. Exp. Med. *198*, 293–303.

Dykstra, B., Kent, D., Bowie, M., McCaffrey, L., Hamilton, M., Lyons, K., Lee, S.-J., Brinkman, R., and Eaves, C. (2007). Long-Term Propagation of Distinct Hematopoietic Differentiation Programs In Vivo. Cell Stem Cell *1*, 218–229.

Ema, H., Morita, Y., and Suda, T. (2014). Heterogeneity and hierarchy of hematopoietic stem cells. Exp. Hematol. *42*, 74–82.e2.

Forsberg, E.C., Serwold, T., Kogan, S., Weissman, I.L., and Passegué, E. (2006). New Evidence Supporting Megakaryocyte-Erythrocyte Potential of Flk2/Flt3+ Multipotent Hematopoietic Progenitors. Cell *126*, 415–426.

Gerrits, A., Dykstra, B., Kalmykowa, O.J., Klauke, K., Verovskaya, E., Broekhuis, M.J.C., de Haan, G., and Bystrykh, L. V (2010). Cellular barcoding tool for clonal analysis in the hematopoietic system. Blood *115*, 2610–2618.

Hock, H. (2010). Some hematopoietic stem cells are more equal than others: Figure 1. J. Exp. Med. *207*, 1127–1130.

Kakumitsu, H., Kamezaki, K., Shimoda, K., Karube, K., Haro, T., Numata, A., Shide, K., Matsuda, T., Oshima, K., and Harada, M. (2005). Transgenic mice overexpressing murine thrombopoietin develop myelofibrosis and osteosclerosis. Leuk. Res. *29*, 761–769.

Kokkaliaris, K.D., Lucas, D., Beerman, I., Kent, D.G., and Perié, L. (2016). Understanding hematopoiesis from a single-cell standpoint. Exp. Hematol. *44*, 447–450.

Kondo, M., Weissman, I.L., and Akashi, K. (1997). Identification of clonogenic common lymphoid progenitors in mouse bone marrow. Cell *91*, 661–672.

Lai, A.Y., and Kondo, M. (2006). Asymmetrical lymphoid and myeloid lineage commitment in multipotent hematopoietic progenitors. J. Exp. Med. *203*, 1867–1873.

Lu, R., Neff, N.F., Quake, S.R., and Weissman, I.L. (2011). Tracking single hematopoietic stem cells in vivo using high-throughput sequencing in conjunction with viral genetic barcoding. Nat. Biotechnol. *29*, 928–933.

Miyawaki, K., Arinobu, Y., Iwasaki, H., Kohno, K., Tsuzuki, H., Iino, T., Shima, T., Kikushige, Y., Takenaka, K., Miyamoto, T., et al. (2015). CD41 Marks the Initial Myelo-Erythroid Lineage Specification in Adult Mouse Hematopoiesis: Redefinition of Murine Common Myeloid Progenitor. Stem Cells *33*, 976–987.

Na Nakorn, T., Traver, D., Weissman, I.L., and Akashi, K. (2002). Myeloerythroid-restricted progenitors are sufficient to confer radioprotection and provide the majority of day 8 CFU-S. J. Clin. Invest. *109*, 1579–1585.

Nemzek, J.A., Bolgos, G.L., Williams, B.A., and Remick, D.G. (2001). Differences in normal values for murine white blood cell counts and other hematological parameters based on sampling site. Inflamm. Res. *50*, 523–527.

Notta, F., Zandi, S., Takayama, N., Dobson, S., Gan, O.I., Wilson, G., Kaufmann, K.B., McLeod, J., Laurenti, E., Dunant, C.F., et al. (2016). Distinct routes of lineage development reshape the human blood hierarchy across ontogeny. Science (80-.).

Nutt, S.L., Metcalf, D., D'Amico, A., Polli, M., and Wu, L. (2005). Dynamic regulation of PU.1 expression in multipotent hematopoietic progenitors. J. Exp. Med. *201*, 221–231.

Oguro, H., Ding, L., and Morrison, S.J. (2013). SLAM family markers resolve functionally distinct subpopulations of hematopoietic stem cells and multipotent progenitors. Cell Stem Cell *13*, 102–116.

Osawa, M., Hanada, K., Hamada, H., and Nakauchi, H. (1996). Long-term lymphohematopoietic reconstitution by a single CD34-low/negative hematopoietic stem cell. Science *273*, 242–245.

Paul, F., Arkin, Y., Giladi, A., Jaitin, D.A., Kenigsberg, E., Keren-Shaul, H., Winter, D., Lara-Astiaso, D., Gury, M., Weiner, A., et al. (2015). Transcriptional Heterogeneity and Lineage Commitment in Myeloid Progenitors. Cell *163*, 1663–1677.

Perié, L., Duffy, K.R., Kok, L., De Boer, R.J., and Schumacher, T.N. (2015). The Branching Point in Erythro-Myeloid Differentiation. Cell.

Pronk, C.J.H., Rossi, D.J., Månsson, R., Attema, J.L., Norddahl, G.L., Chan, C.K.F., Sigvardsson, M., Weissman, I.L., and Bryder, D. (2007). Elucidation of the Phenotypic, Functional, and Molecular Topography of a Myeloerythroid Progenitor Cell Hierarchy. Cell Stem Cell *1*, 428–442.

Richie Ehrlich, L.I., Serwold, T., and Weissman, I.L. (2011). In vitro assays misrepresent in vivo lineage potentials of murine lymphoid progenitors. Blood *117*, 2618–2624.

Rodriguez-Fraticelli, A.E., Wolock, S.L., Weinreb, C.S., Panero, R., Patel, S.H., Jankovic, M., Sun, J., Calogero, R.A., Klein, A.M., and Camargo, F.D. (2018). Clonal analysis of lineage fate in native haematopoiesis. Nature.

Schaefer, B.C., Schaefer, M.L., Kappler, J.W., Marrack, P., and Kedl, R.M. (2001). Observation of Antigen-Dependent CD8+ T-Cell/ Dendritic Cell Interactions in Vivo. Cell. Immunol. *214*, 110–122.

Schlenner, S.M., Madan, V., Busch, K., Tietz, A., Läufle, C., Costa, C., Blum, C., Fehling, H.J., and Rodewald, H.R. (2010). Fate Mapping Reveals Separate Origins of T Cells and Myeloid Lineages in the Thymus. Immunity *32*, 426–436.

Schroeder, T. (2010). Hematopoietic Stem Cell Heterogeneity: Subtypes, Not Unpredictable Behavior. Cell Stem Cell *6*, 203–207.

Smith-Berdan, S., Nguyen, A., Hassanein, D., Zimmer, M., Ugarte, F., Ciriza, J., Li, D., García-Ojeda, M.E., Hinck, L., and Forsberg, E.C. (2011). Robo4 cooperates with CXCR4 to specify hematopoietic stem cell localization to bone marrow niches. Cell Stem Cell *8*, 72–83.

Smith-Berdan, S., Nguyen, A., Hong, M.A., and Forsberg, E.C. (2015). ROBO4-mediated vascular integrity regulates the directionality of hematopoietic stem cell trafficking. Stem Cell Reports *4*, 255–268.

Sun, J., Ramos, A., Chapman, B., Johnnidis, J.B., Le, L., Ho, Y.J., Klein, A., Hofmann, O., and Camargo, F.D. (2014). Clonal dynamics of native haematopoiesis. Nature *514*, 322–327.

Ugarte, F., Sousae, R., Cinquin, B., Martin, E.W., Krietsch, J., Sanchez, G., Inman, M., Tsang, H., Warr, M., Passegué, E., et al. (2015). Progressive Chromatin Condensation and H3K9 Methylation Regulate the Differentiation of Embryonic and Hematopoietic Stem Cells. Stem Cell

Reports *5*, 728–740.

Weber, K., Thomaschewski, M., Warlich, M., Volz, T., Cornils, K., Niebuhr, B., Täger, M., Lütgehetmann, M., Pollok, J.-M., Stocking, C., et al. (2011). RGB marking facilitates multicolor clonal cell tracking. Nat. Med. *17*, 504–509.

Yamamoto, R., Morita, Y., Ooehara, J., Hamanaka, S., Onodera, M., Rudolph, K.L., Ema, H., and Nakauchi, H. (2013). Clonal analysis unveils self-renewing lineage-restricted progenitors generated directly from hematopoietic stem cells. Cell *154*, 1112–1126.

Yamamoto, R., Wilkinson, A.C., Ooehara, J., Lan, X., Lai, C.Y., Nakauchi, Y., Pritchard, J.K., and Nakauchi, H. (2018). Large-Scale Clonal Analysis Resolves Aging of the Mouse Hematopoietic Stem Cell Compartment. Cell Stem Cell *5*; 600-607.

FIGURE TITLES AND LEGENDS

Figure 1. Reconstitution potential of transplanted hematopoietic stem and progenitor cell populations.

(**A-G**) Percent donor chimerism over 110 days from HSCs (**A**), MPP^F (**B**), CMPs (**C**), CMP^F (**D**), GMPs (**E**), MEPs (**F**), or CLP^F (**G**) upon transplantation into sublethally irradiated (500 rad) mice.

(**H**) B cell numbers display a rapid and more drastic decline (1,000-fold) after sublethal irradiation than other mature cell types (1.4-, 6-, 6-, and 23-fold for RBCs, Plts, GM and T cells, respectively). Data displayed are fold changes in mature cell numbers in the PB of sublethally irradiated (500 rad) mice over time. n≥7.

(**I**) The number of mature hematopoietic cells in a microliter of peripheral blood (PB) at steady-state. n=10.

(**J**) The distribution of mature hematopoietic cells between blood, bone marrow, spleen, thymus, and lymph nodes of a mouse. n=10.

(**K**) The composition of mouse blood, bone marrow, spleen, thymus, and lymph nodes displayed as a percentage of total mature hematopoietic cells. n=10.

(**L**) The number of mature hematopoietic cells in a 25 gram mouse at steady-state. n=10.

(**M-S**) Reconstitution data from **A-G** replotted as the absolute number of donor-derived cells per microliter PB. Transplantation data in **A-G** and **M-S** are representative means ± SEM from at least 7 recipient mice per cell type from at least two independent experiments. See also Figures S1 and S2.

Figure 2. Comparative mature cell accumulation and kinetics by transplanted hematopoietic stem and progenitor cell populations.

(**A-E**) The total number of RBCs (**A**), Plts (**B**), GMs (**C**), B-cells (**D**), and T-cells (**E**) present per mouse per transplanted HSPC.

(**A'-E'**) The approximate timepoint and cell number for peak donor-derived mature cells from **A-E**.

Data were generated from the transplantation and cell distribution experiments of Figure 1. The mature cell production capacity was always in the same order: HSCs > MPP^F > CLP^F (for B and T cells) and HSCs > MPP^F > CMP > CMP^F > MEP > GMP (for RBCs, Plts, and GM cells). The only exception was that significantly more GM cells accumulated after CMP^F than CMP transplantation (**C** and **C'**; $p<0.0009$ by Student's two-tailed t-test). All other comparisons were also significant. See also Figure S3.

Figure 3. Both HSCs and MPP^F generate all types of erythromyeloid progenitors after transplantation.

(**A**) Schematic of HSC and MPP^F transplantation from UBC-GFP mice, short-term analysis of donor-derived progenitor cells, and subsequent functional analysis of the same donor-derived progenitor cells by secondary transplantation.

(**B-I**) Analysis of donor-derived cells in the BM of recipients shortly after transplantation of HSCs and MPP^F. Cells were pre-gated on GFP+ to only display donor-derived cells.

(**B-C**) At Day 2 post-transplantation, the phenotype of GFP+ cells in the BM of sublethally irradiated (500 rad) recipient mice was predominantly the same as the phenotype of the input cell type.

(**D,E,H**) Transplanted HSCs gave rise to phenotypic classical CMP, GMP and MEP (**D^1-D^2**); progenitors defined by alternative markers as MkP, "GMP", pre-GM, pre-EP, pre-CFU-E and pre-MegE (**E^1-E^2**); and EP and GM cells (**H^1-H^2**) by days 7 and 14 post-transplantation into

lethally irradiated (1,000 rad) recipients. Few HSC-derived B and T cells were observed at these timepoints (**H^1-H^2**).

(**F,G,I**) Transplanted MPP^F gave rise to phenotypic classical CMP, GMP and MEP (**F^1-F^4**); MkP, "GMP", pre-GM, pre-EP, pre-CFU-E and pre-MegE (**G^1-G^4**); and EP, GM, B and T cells (**I^1-I^4**) by days 4, 7, 11 and 14 post-transplantation.

(**$D^{1'}$-$I^{4'}$**) Quantification of results displayed in panels **D-I** demonstrated substantial expansion in donor-derived cell numbers during the course (4-14 days) of the experiments. Most comparisons of the absolute cell numbers between time points and between HSCs and MPP^F were significantly different; however, the proportions of progenitor cells generated were similar. For example, both HSCs and MPP^F generated more GMPs than MEPs and CMPs, and the proportions of CMP/GMP/MEP generated by HSCs at day 11 and MPP^F at day 14 were not significantly different from each other (Student's two-tailed t-test for HSCs; one-way ANOVA with multiple post-hoc comparisons for MPP^Fs; **$D^{1'}$-$I^{4'}$**). n=3 or more recipients in 2 or more independent experiments for each donor cell type and analysis timepoint. Data are displayed as means ± SEM. Abbreviations for pregating of panels H^1-I^4: Ery, TER-119; Ly, CD3 and B220; My, Gr1 and Mac1. *p<0.05, **p<0.01, ***p<0.001. See also Figure S4.

Figure 4. Single HSCs and MPP^F reconstituted both myeloid and lymphoid lineages *in vivo*.

(**A**) Alternative models of MPP^F multipotency. The multilineage reconstitution by MPP^F transplanted in bulk (Figures 1B and 1N) may be derived from clonally multipotent MPP^F (left panel) or from the combined contribution of lineage-committed cells with a shared MPP^F surface phenotype (right panel).

(**B**) Summary of the results from single transplanted HSCs and from single and multiple MPP^F. P=0.05 for 1 HSC versus 25 MPP^F; P>0.1 for 1 HSC versus 5 MPP^F; P<0.05 for 1 HSC versus 1 MPP^F by chi-squared test of independence in reconstitution patterns.

(**C-F**) Lineages detected in individual lethally irradiated (1,000 rad) recipients receiving either single HSCs or 1, 5 or 25 MPP^F. Mature cell detection by flow cytometry is indicated for each recipient and cell type by a filled square (RBCs, red; Plts, pink; GMs, orange; B cells, blue; T cells, teal).

(**G-J**) Percent donor chimerism and (**K-N**) distribution of mature cells from single HSCs and 25, 5 or single MPP^F. Representative recipients that displayed multilineage reconstitution are shown.

(**O**) B cell numbers display a rapid and more drastic decline (2,000-fold) after lethal irradiation than other mature cell types (4- to 150-fold for RBCs and T cells, respectively). Data displayed are fold change in mature cell numbers in the PB of lethally irradiated (1,000 rad) mice over time. n=4.

(**P-T**) The magnitude and timing of host cell depletion and recovery affects the ability to detect reconstitution from transplanted progenitor cells. Numbers from panel (**O**) superimposed with the kinetics of mature cell generation by HSCs and MPP^F for each lineage, displayed relative to the peak reconstitution (set at 1.00) for each population.

All data are from at least three independent experiments. See also Figures S5 and S6.

Figure 5. Multilineage reconstitution by single HSCs and MPP^F in *in vivo* spleen colony assays.

(**A**) In support of the clonal origin of spleen colonies, CFU-S were comprised of only a single color, either red or green, after transplantation of a mixture of Tomato+ and GFP+ cells. Representative fluorescent microscopy images are shown.

(**B-F**) Spleen colonies derived from single HSCs or MPP^F contain erythroid, megakaryocytic, GM, and B-cell lineages. Donor cells from UBC-GFP mice were transplanted into lethally irradiated (1,000 rad) mice. CFU-S were dissected and analyzed by flow cytometry at the timepoint post-transplantation of largest colony size; HSCs on day 13.5 (n=13), MPP^F on day 11.5 (n=18), CMPs on day 9.5 (n=16), CMP^F on day 9.5 (n=8), and MEPs on day 8.5 (n=9).

(**B**) Gating strategy and analysis of a representative MPP^F-derived CFU-S. The percentages of donor-derived (GFP+) cells for each cell type within representative colonies are shown in the histograms on the right, with gating strategies shown on the left.

(**C**) Substantially lower donor contribution was observed in the PB (**C**) than within CFU-S (**B**), indicating that the detection of multiple lineages within a colony is not due to contamination of circulating cells. Of note, there were no detectable EPs or Megs in the PB. Representative flow cytometry plots are from a recipient of MPP^F.

(**D**) Proportion of individual CFU-S containing detectable erythroid progenitors (EPs), megakaryocytes (Meg), GM, and/or B cells.

(**E**) Summary of the CFU-S data shown in panel **D**. The colony type distribution was not significantly different for HSCs versus MPP^F ($p > 0.1$; chi-squared test of independence).

(**F**) The frequency of EPs, Meg, GM and B cells in dissected CFU-S colonies from (**D**). Percentages are shown as donor-derived (GFP+) cells only.

Data represent 4 independent experiments with a total of 12-17 mice per group. *$p<0.05$, **$p<0.01$, ***$p<0.001$ by unpaired t-test.

Figure 6. Hematopoietic differentiation model where erythroid production represents the default fate of HSCs. Both functional experiments and gene expression data indicate that the capacity to generate RBCs and Plts is acquired upon specification of HSCs from a hematovascular precursor. Despite downregulation of genes that drive MegE development,

RBC and Plt production remain the predominant fates of MPP^F and other non-lymphoid committed progenitors. Relatively rare production of GM, B and T cells occurs through combined downregulation of MegE drivers and a gain of gene products promoting the alternative fates. Initiation of non-MegE fates in MPP^F may thus be viewed as gain of GM and lymphoid potential, rather than loss of capacity to generate RBCs and/or Plts.

TABLES

Table 1. Approximate proportion of the absolute number of mature cells generated by each transplanted progenitor cell type. nd, not detected. See also Tables S1 and S2.

	RBC	Plt	GM	B	T
HSC	86.2	7.22	2.87	2.48	1.25
MPP^F	98.3	0.56	0.47	0.31	0.33
CMP	99.7	0.26	0.01	nd	nd
CMP^F	99.4	0.29	0.31	nd	nd
GMP	90.8	0.79	8.37	nd	nd
MEP	99.9	0.12	nd	nd	nd
CLP	nd	nd	nd	91	9

Figure 1

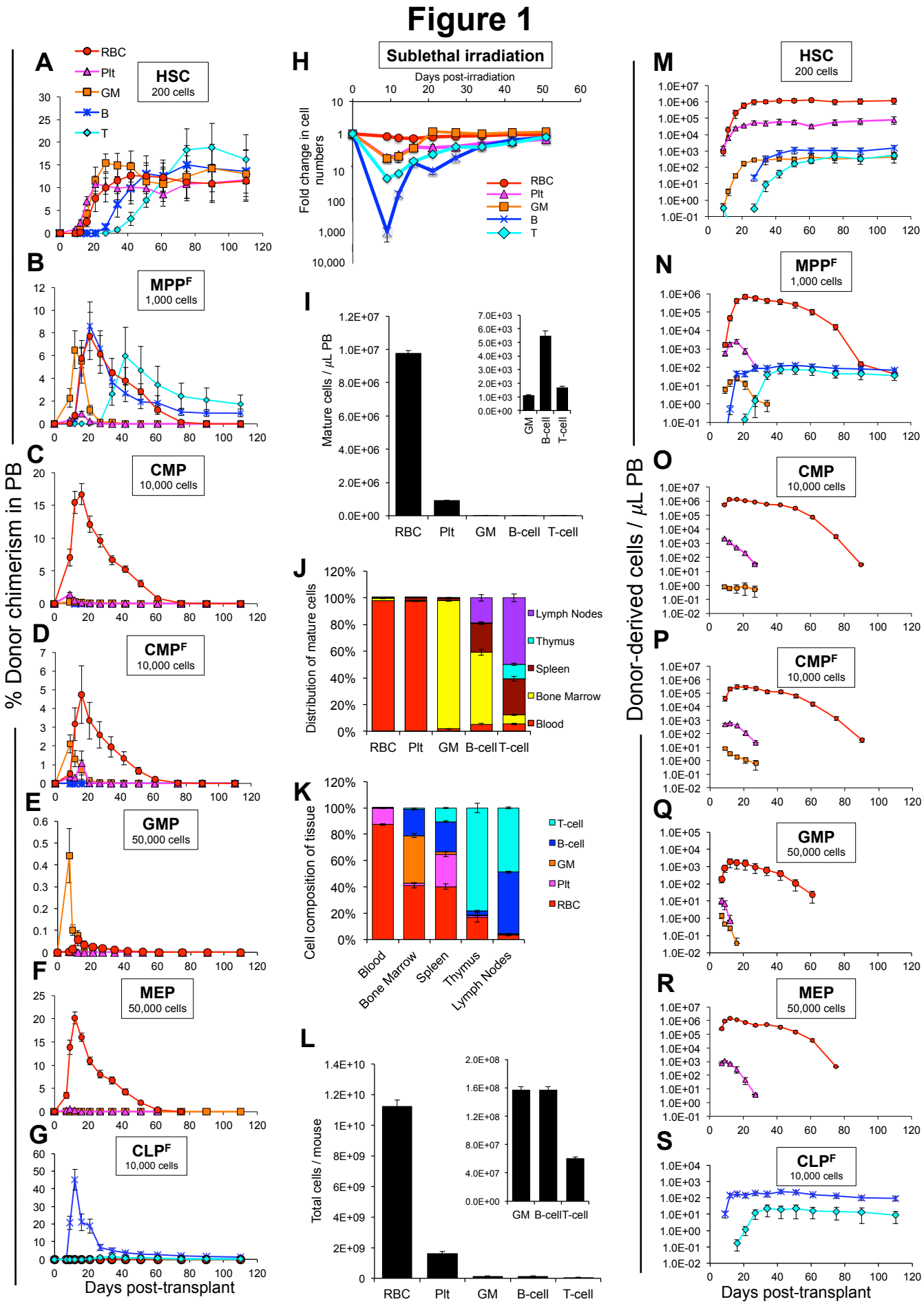
Figure 1
A
HSC
200 cells
RBC
Plt
GM
B
T
B
MPP^F
1,000 cells
C
CMP
10,000 cells
D
CMP^F
10,000 cells
E
GMP
50,000 cells
F
MEP
50,000 cells
G
CLP^F
10,000 cells
Days post-transplant
% Donor chimerism in PB
H
Sublethal irradiation
Days post-irradiation
Fold change in cell numbers
I
Mature cells / μL PB
RBC Plt GM B-cell T-cell
J
Distribution of mature cells
Lymph Nodes
Thymus
Spleen
Bone Marrow
Blood
K
Cell composition of tissue
T-cell
B-cell
GM
Plt
RBC
Blood Bone Marrow Spleen Thymus Lymph Nodes
L
Total cells / mouse
M
HSC
200 cells
N
MPP^F
1,000 cells
O
CMP
10,000 cells
P
CMP^F
10,000 cells
Q
GMP
50,000 cells
R
MEP
50,000 cells
S
CLP^F
10,000 cells
Donor-derived cells / μL PB
Days post-transplant

Figure 2

Figure 2

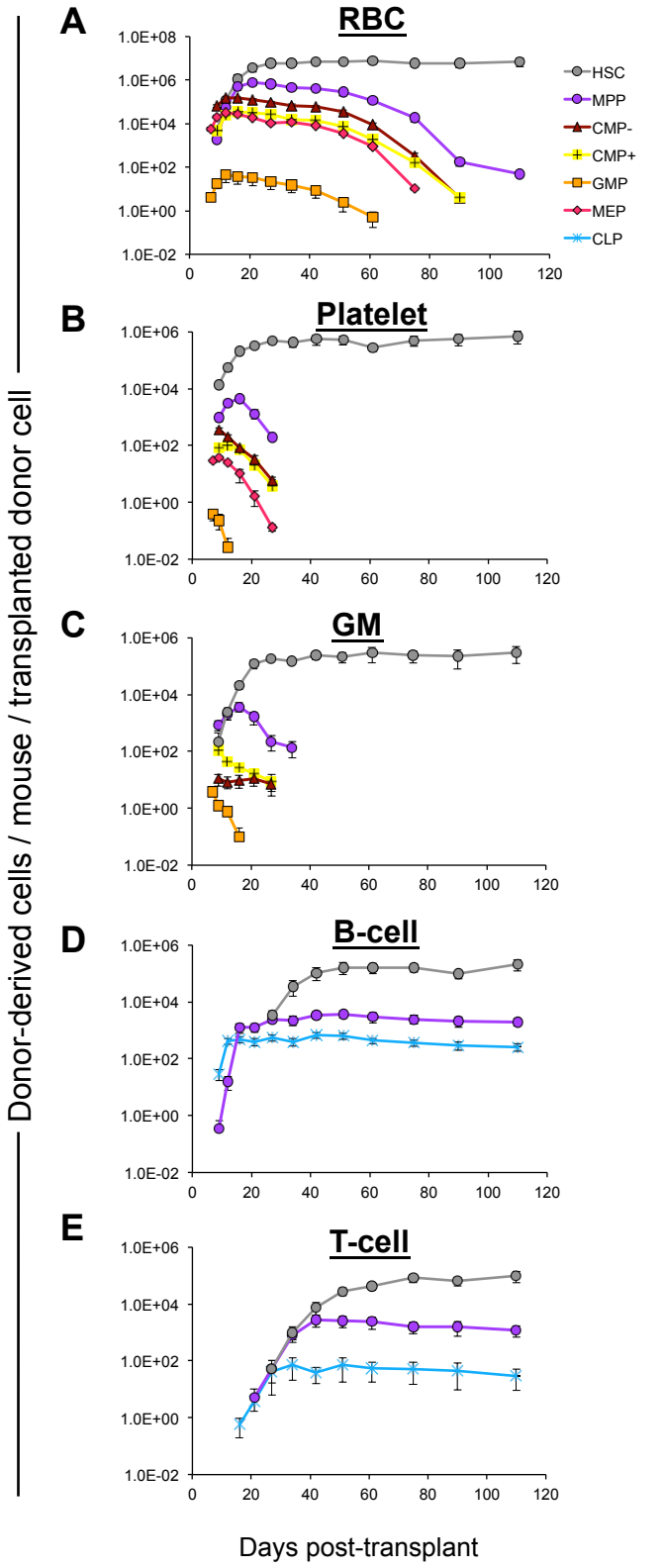

A'

	Day of peak	No. cells at peak
HSC	27 +	5.6E6 (±1.8E6)
MPP^F	21	7.9E5 (±2.4E5)
CMP	12	1.4E5 (±1.8E4)
CMP^F	16	3.5E4 (±1.3E4)
GMP	12	4.3E1 (±2.3E1)
MEP	12	3.2E4 (±3.2E3)
CLP^F	N/A	N/A

CMP > CMP^F p=0.0001

B'

	Day of peak	No. cells at peak
HSC	27 +	4.7E5 (±1.1E5)
MPP^F	16	4.5E3 (±1.0E3)
CMP	9	3.7E2 (±5.2E1)
CMP^F	12	1.0E2 (±1.6E1)
GMP	7	3.7E-1 (±1.5E-1)
MEP	9	3.9E1 (±2.8E0)
CLP^F	N/A	N/A

CMP > CMP^F p=0.0001

C'

	Day of peak	No. cells at peak
HSC	27 +	1.9E5 (±2.3E4)
MPP^F	16	3.7E3 (±1.3E3)
CMP	9	1.1E1 (±4.8E0)
CMP^F	9	1.1E2 (±2.4E1)
GMP	7	3.9E0 (±1.3E0)
MEP	N/A	N/A
CLP^F	N/A	N/A

CMP^F > CMP p=0.0009

D'

	Day of peak	No. cells at peak
HSC	51 +	1.6E5 (±7.3E4)
MPP^F	27	2.5E3 (±6.9E2)
CMP	N/A	N/A
CMP^F	N/A	N/A
GMP	N/A	N/A
MEP	N/A	N/A
CLP^F	12	4.2E2 (±1.0E2)

E'

	Day of peak	No. cells at peak
HSC	75 +	8.2E4 (±2.6E4)
MPP^F	42	2.7E3 (1.2E3)
CMP	N/A	N/A
CMP^F	N/A	N/A
GMP	N/A	N/A
MEP	N/A	N/A
CLP^F	27	4.2E1 (±2.5E1)

Figure 3

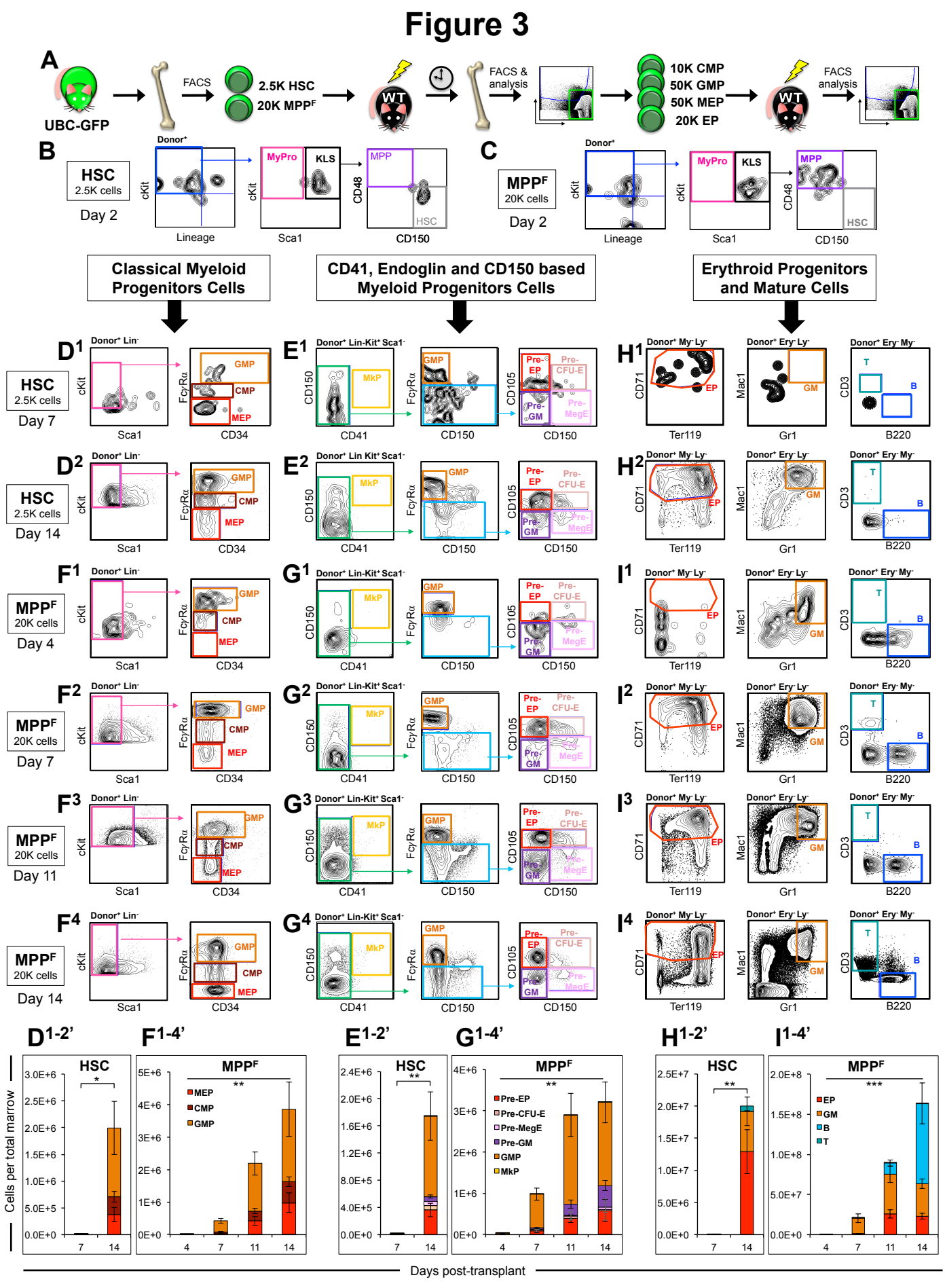
Figure 3
A
UBC-GFP
FACS
2.5K HSC
20K MPPF
WT
FACS & analysis
10K CMP
50K GMP
50K MEP
20K EP
WT
FACS analysis
B
HSC
2.5K cells
Day 2
Donor+
cKit
Lineage
MyPro
KLS
Sca1
MPP
HSC
CD48
CD150
C
MPPF
20K cells
Day 2
Classical Myeloid Progenitors Cells
CD41, Endoglin and CD150 based Myeloid Progenitors Cells
Erythroid Progenitors and Mature Cells
D1
HSC
2.5K cells
Day 7
Donor+ Lin-
GMP
CMP
MEP
FcγRα
CD34
E1
Donor+ Lin-Kit+ Sca1-
MkP
CD41
CD150
Pre-EP
Pre-CFU-E
Pre-GM
Pre-MegE
CD105
H1
Donor+ My-Ly-
CD71
EP
Ter119
Donor+ Ery-Ly-
Mac1
GM
Gr1
Donor+ Ery-My-
CD3
T
B
B220
D2
HSC
2.5K cells
Day 14
E2
H2
F1
MPPF
20K cells
Day 4
G1
I1
F2
MPPF
20K cells
Day 7
G2
I2
F3
MPPF
20K cells
Day 11
G3
I3
F4
MPPF
20K cells
Day 14
G4
I4
D1-2'
F1-4'
E1-2'
G1-4'
H1-2'
I1-4'
HSC
MPPF
Cells per total marrow
MEP
CMP
GMP
Pre-EP
Pre-CFU-E
Pre-MegE
Pre-GM
MkP
EP
GM
B
T
Days post-transplant

Figure 4

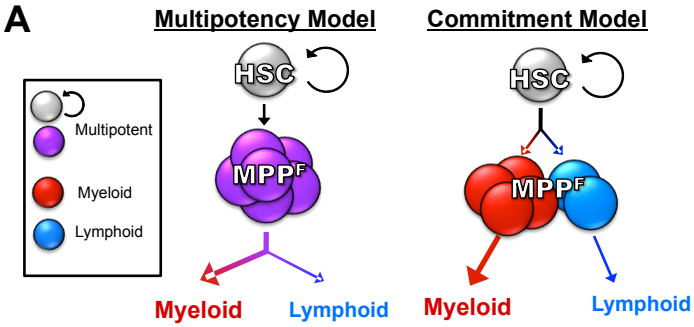

B

	no. pos. mice / total mice transplanted	Myeloid+ Lymphoid	Myeloid only	Lymphoid only
1 HSC	20/108 (19%)	11/20 (55%)	9/20 (45%)	0/20 (0%)
1 MPP^F	21/121 (17%)	9/21 (43%)	5/21 (24%)	7/21 (33%)
5 MPP^F	24/41 (59%)	9/24 (37.5%)	12/24 (50%)	3/24 (12.5%)
25 MPP^F	9/9 (100%)	9/9 (100%)	0/9 (0%)	0/9 (0%)

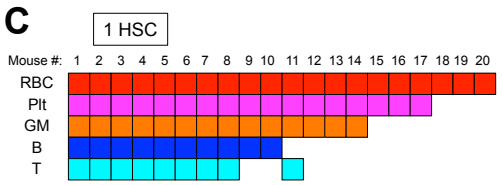

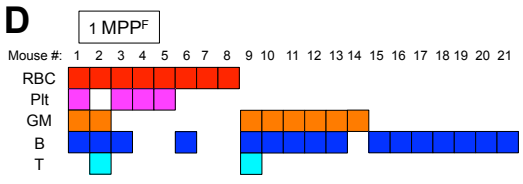

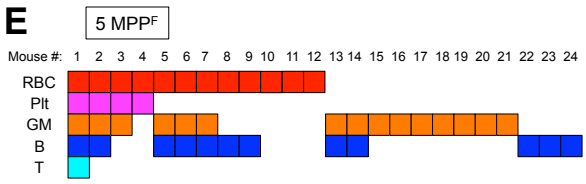

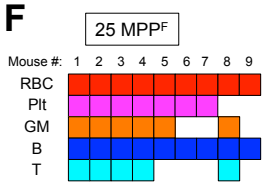

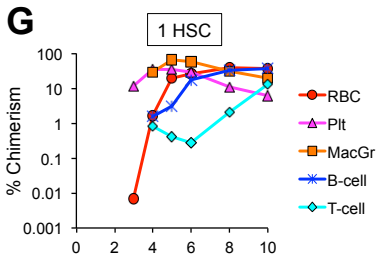

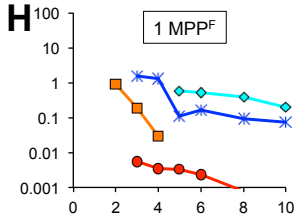

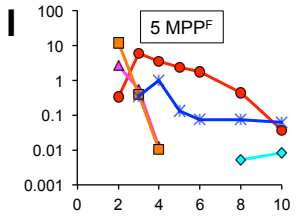

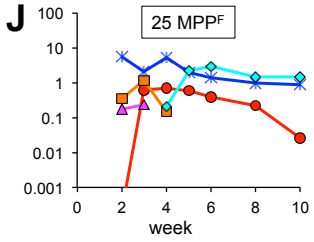

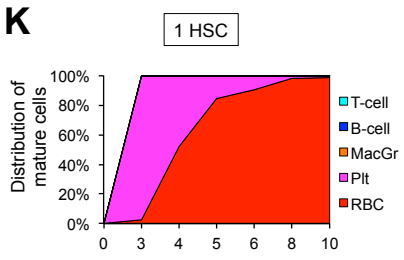

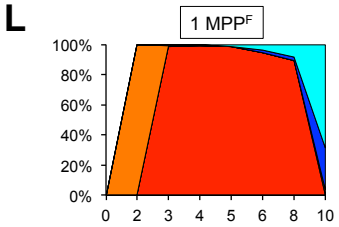

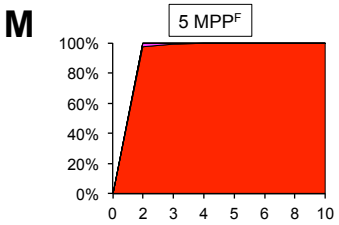

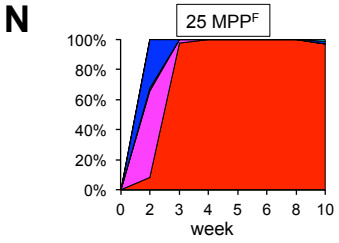

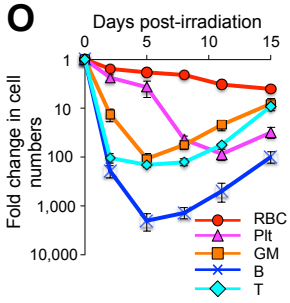

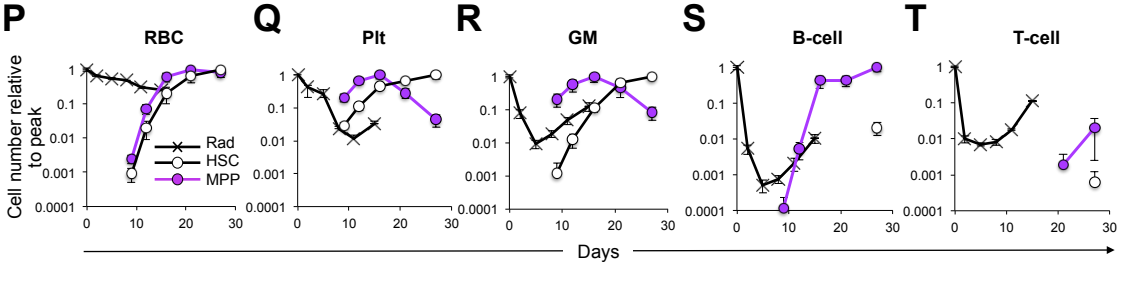

Figure 5

Figure 5

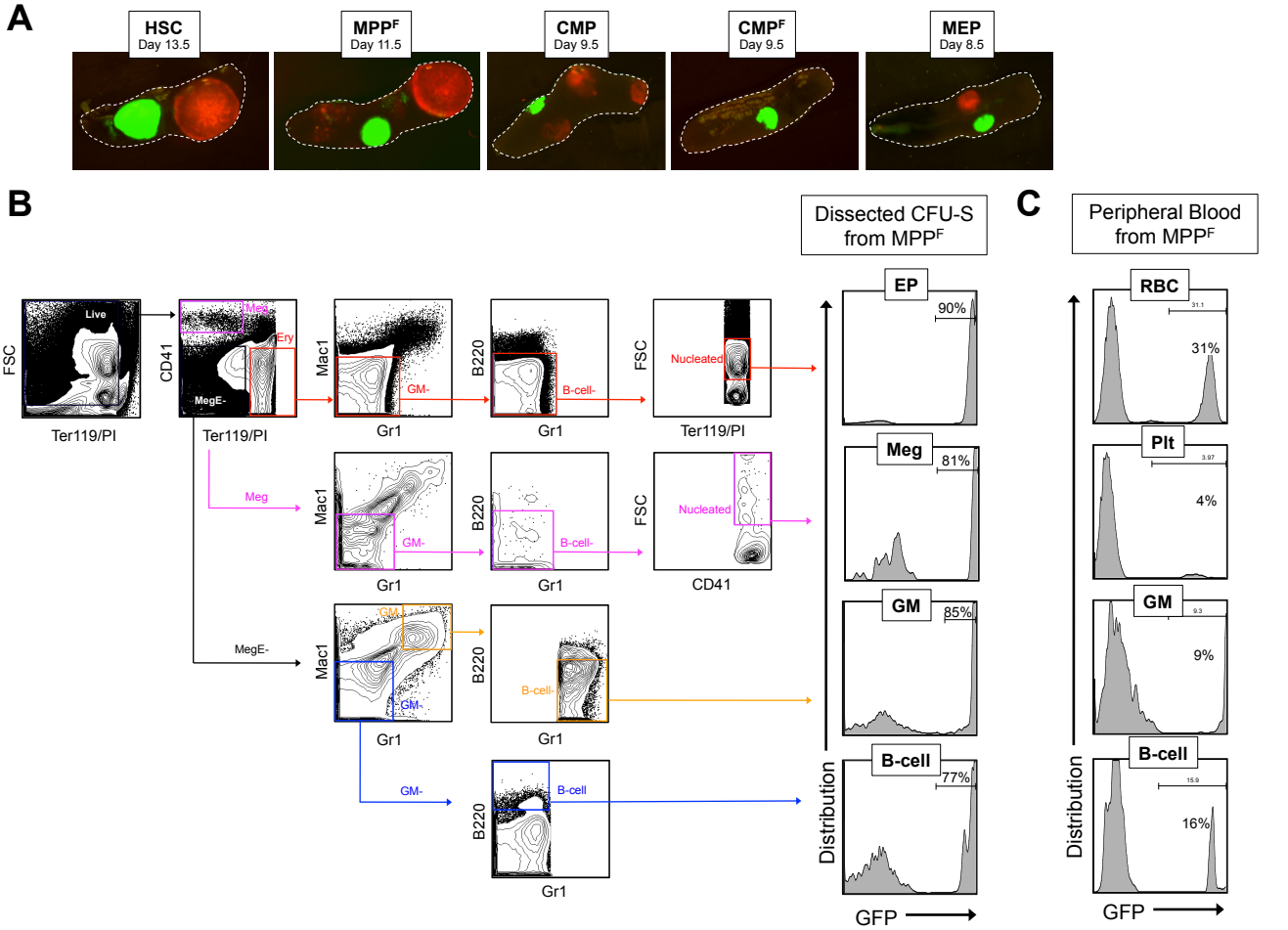

	Myeloid + Lymphoid CFU-S	Myeloid only CFU-S	Lymphoid only CFU-S
HSC	46% (6/13)	54% (7/13)	0% (0/13)
MPP^F	67% (12/18)	33% (6/18)	0% (0/18)

Figure 6

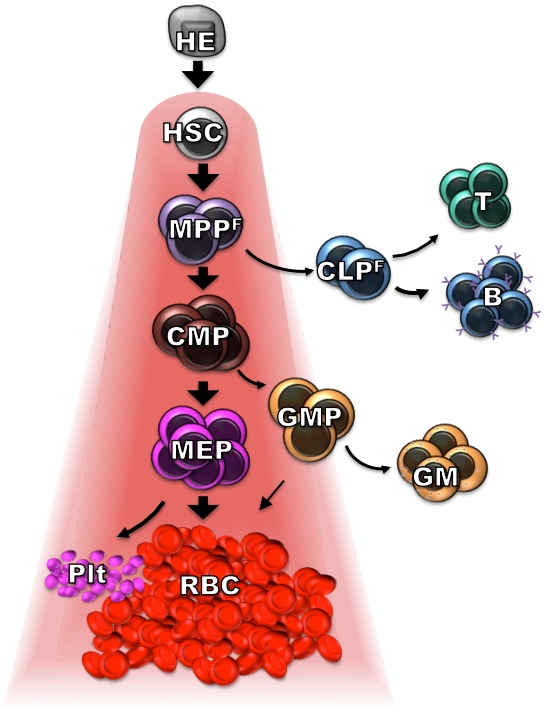

SUPPLEMENTAL TABLE 1

	RBC	Plt	GM	B	T
HSC	51.2	16.1	31.2	0.91	0.27
MPP^F	96.1	0.73	2.30	0.56	0.28
CMP	99.7	0.20	0.07	nd	nd
CMP^F	98.8	0.37	0.85	nd	nd
GMP	87.2	0.68	12.1	nd	nd
MEP	99.9	0.13	nd	nd	nd
CLP	nd	nd	nd	92.4	7.6

Supplemental Table 1: Proportion of each mature cell type generated from each progenitor cell population during the entire 110 day time course of the transplantation experiments in Figure 1 calculated using an “extreme half-life” scenario (illustrated in Figure S3).

SUPPLEMENTAL TABLE 2

	Total numbers of cells	
Cell type	Burst phase method	Extreme half-life method
HSC	6,502,000	48,496,584
MPP^F	803,400	1,035,218
CMP	140,380	188,077
CMP^F	35,210	45,467
GMP	47	54
MEP	32,029	39,002
CLP	462	1,189

Supplemental Table 2: The estimated numbers of total cells produced per transplanted stem/progenitor cell are similar whether derived by the “burst phase” method or by the “extreme half-life” method (illustrated in Figure S3). The “burst phase method” was used as in Figure 2 and Table 1 of the manuscript and the “extreme half-life” method in Figure S2A’-G’, and Table S1. Because progenitors only produce significant numbers of new cells during the burst phase, the two methods largely agree. This is not true for HSCs, as they self-renew and give rise to an indefinite number of cells.

Supplemental Figure 1

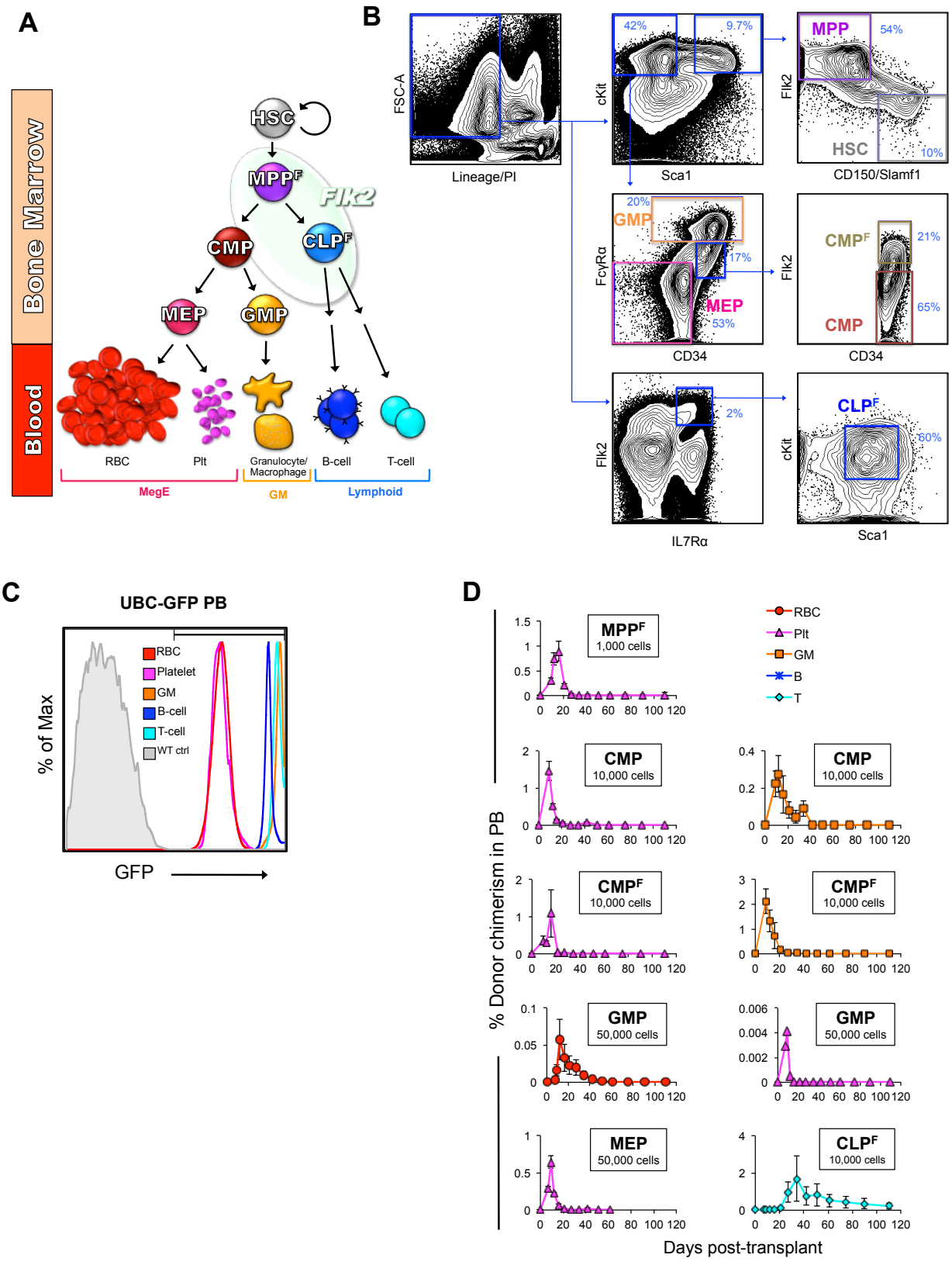

Supplemental Figure 1: Transplantation strategy for evaluating lineage potentials from various HPSCs double-sorted from UBC-GFP mice.

(**A**) Schematic of hematopoietic differentiation to illustrate the terminology used for cell types and lineages in the text.

(**B**) FACS-sorting strategy for isolating hematopoietic subtypes. Cells were pre-gated for singlets only (FSC-W^{low}). Bone marrow was cKit-enriched prior to FACS-sorting of transplanted cell types, with the exception of CLPs where lineage-depletion was used instead of cKit enrichment.

(**C**) Flow cytometry analysis of peripheral blood (PB) cells from UBC-GFP mice showing high levels of GFP expression in both nucleated and enucleated hematopoietic cell types.

(**D**) Reconstitution data from Figure 1B-G, replotted as separate, mature donor-derived cells on different y-axis scales to visualize lineages with low levels of donor chimerism.

HSC – Hematopoietic Stem Cell; MPP^F – Multipotent Progenitor; CMP – Common Myeloid Progenitor; CMP^F – FLK2+ Common Myeloid Progenitor; CLP^F – Common Lymphoid Progenitor; GMP – Granulocyte/Myelomonocyte Progenitor; MEP – Megakaryocyte/Erythrocyte Progenitor; RBC - Red Blood Cell; Plt - Platelet; GM - Granulocyte/Myelomonocyte.

Supplemental Figure 2

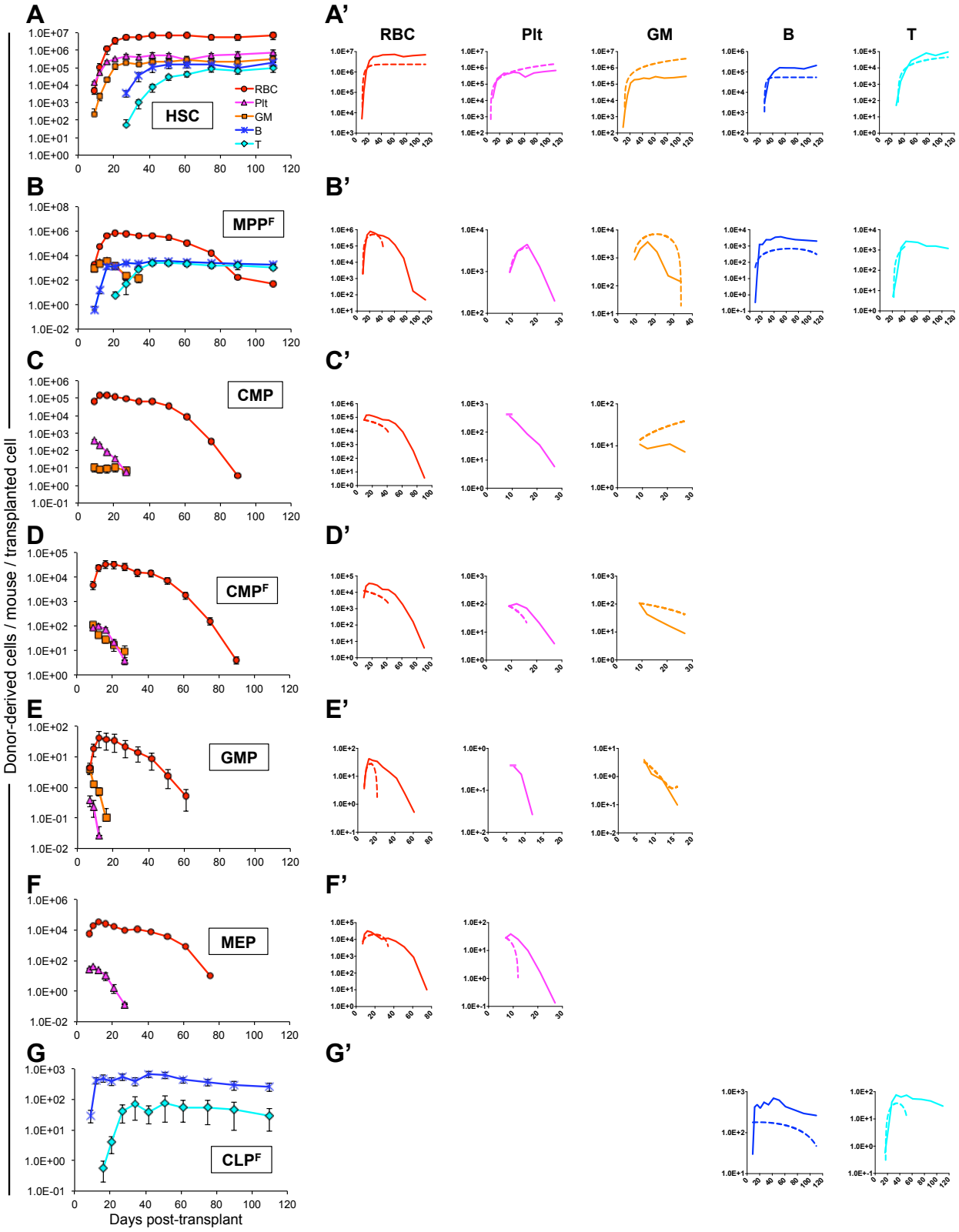

Supplemental Figure 2: Total numbers of mature cells generated per transplanted cell. (**A-G**) Absolute number of donor-derived mature cells present in a mouse over time post-transplantation per transplanted donor cell. Enumeration of donor-derived mature cells in **Figure 1M-S** was used in combination with total mature cell number in the PB (**Figure 1I**) and mature cell distribution (**Figure 1J**) to estimate the total number of mature cells in the entire recipient derived from each HSPC after transplantation.

(**A'-G'**) Calculated absolute number of donor-derived mature cells generated in a mouse over time post-transplantation per transplanted donor cell based on an "extreme half-life" Markov Modeling approach. The numbers in panels A-G were used to estimate new mature cells generated by accounting for the differential half-life, and therefore different extents of cell accumulation, of the different mature cell types. The individual plots for RBCs, Plts, GM, B and T cells provide a side-by-side comparison of "cells present" (solid lines, from the A-G data in the left column) versus "new cells produced" (dashed lines; from the Markov-transformed data) by each transplanted HSC or progenitor cell, as indicated. The solid lines end when the number of donor-derived cells in the peripheral blood approaches zero (or for HSCs, when the experiment was ended). The dashed lines end when new cell production ceased. Note that cells with a shorter half-life (such as GMs) are newly produced at a higher rate than apparent from the "cells present" data (dashed lines are above solid lines), whereas cells with longer half-lives (such as RBCs) accumulate (solid lines are above dashed lines).

Supplemental Figure 3

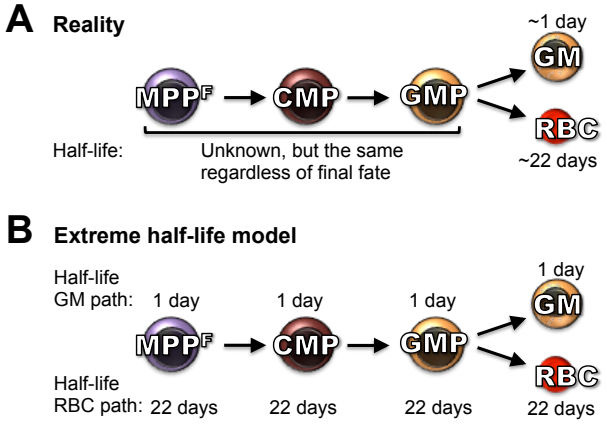

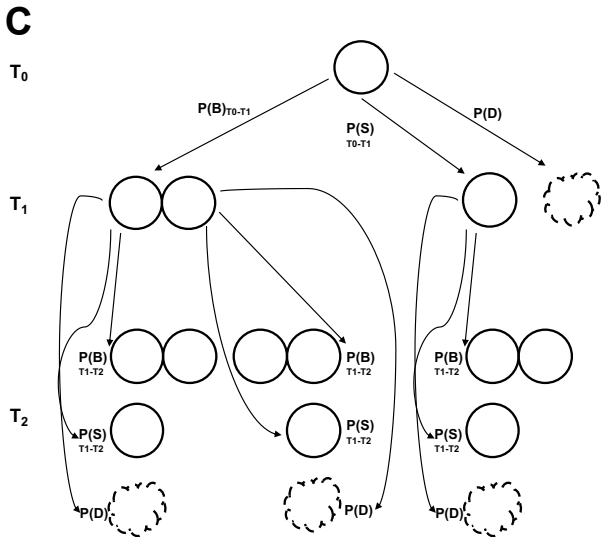

Supplemental Figure 3: Cartoon to illustrate the "extreme half-life" scenario.

(**A**) We know that the approximate half-lives of mature hematopoietic cells vary many fold, but we do not know the half-life of progenitor populations. We also do not know the exact path of differentiation; a hypothetical example of MPPs giving rise to GMs and RBCs via CMPs and GMPs is given to illustrate the concept. In Markov-based calculations to estimate "new mature cells produced", we used the "extreme half-life" scenario (**B**) where we assigned all progenitors of RBCs a 22-day half-life, and all the progenitors of GMs a 1-day half-life, etc. This exaggerates the differences between the "new" and "accumulated" cells, yet the proportions (Table S1) and total numbers (Table S2) of cells produced/accumulated by each progenitor cell lead to very similar conclusions.

(**C**) Schematic of probabilities in the Modified Markov birth/death model. $P(B)_t$, time-dependent probability of birth; P(D), probability of death (calculated based on published half-lives for each mature cell type); $P(S)_t$ probability of no change ($P(S)_t = 1-P(B)_t -P(D)$).

Supplemental Figure 4

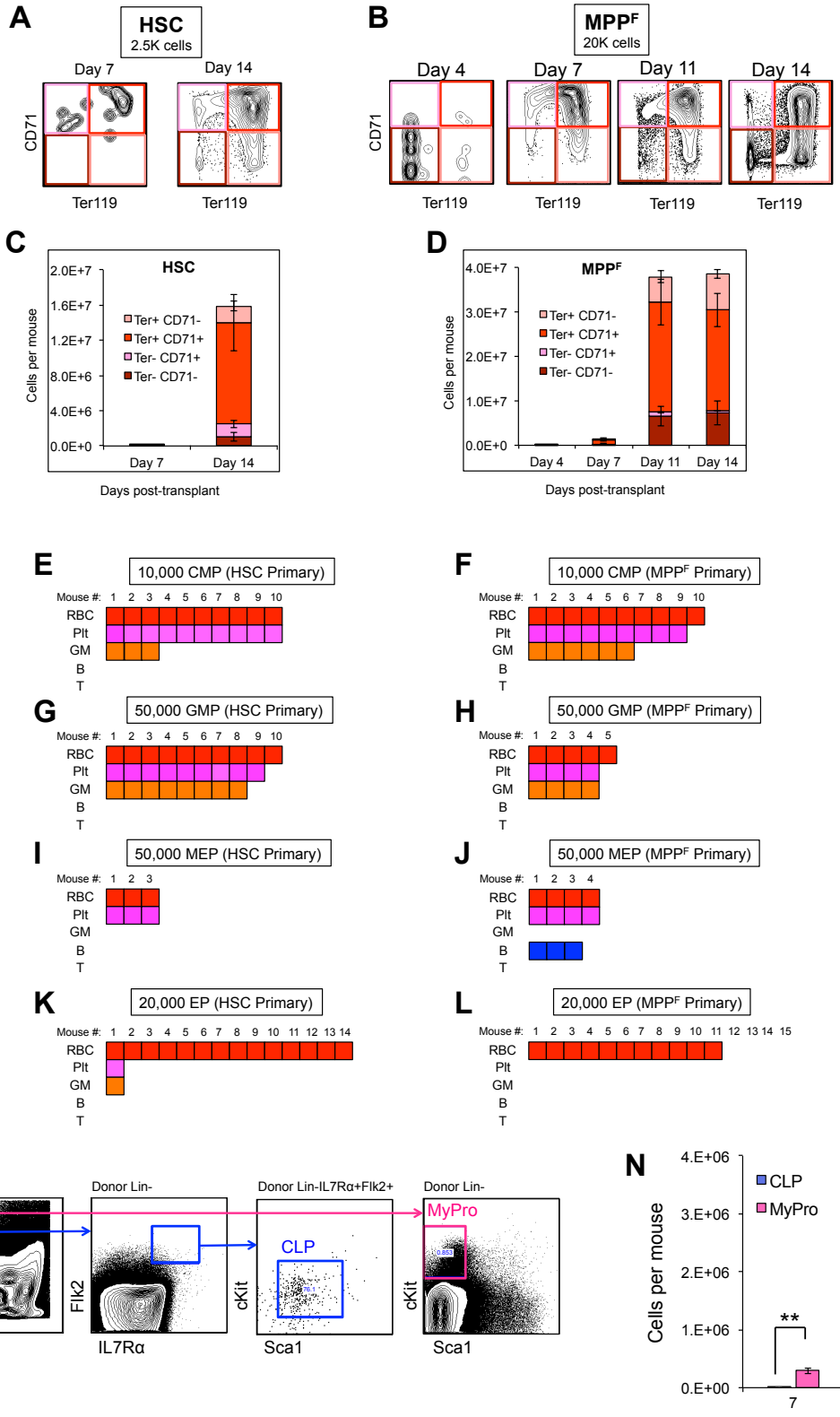

Supplemental Figure 4: Quantification and functional assessment of HSC- and MPP^F-derived progenitor cells.

(**A-B**) Sub-fractionation of donor-derived $Gr1^-Mac1^-B220^-CD3^-$ cells displayed in Figure 4 H^1-$I^{4'}$ by CD71 and TER-119. HSCs and MPP^Fs give rise to all four populations, and the proportions of cells generated by HSCs and MPP^F are similar. Analyses were performed after 4, 7, 11 and 14 days of 2,500 HSCs (A) or 20,000 MPP^Fs (B) transplantation into lethally irradiated hosts.

(**C-D**) Quantification of results displayed in A-B. n=4 to 9 recipients in at least 2 independent experiments (HSC and MPP^F).

(**E-L**) Functional testing by secondary transplantation of progenitor cells produced by HSCs and MPP^Fs in Figure 4 show that these phenotypic progenitor cells have similar functional properties as in primary transplantation. Mature cell detection by flow cytometry is indicated for each recipient and cell type by a filled square (RBCs, red; Plts, pink; GMs, orange; B cells, blue; T cells, teal). Three independent experiments are shown with the number of individual recipients indicated for each transplanted cell type.

(**M-N**) Transplanted MPP^F give rise to higher numbers of myeloid than lymphoid progenitors shortly after transplantation. MPP^F (20,000 cells per recipient) were transplanted into lethally irradiated recipients, followed by analysis of myeloid and lymphoid progenitors in the BM at 7 and 14 days after transplantation. n=4-6 recipients in 3 independent experiments for each analysis timepoint. Data are displayed as means ± SEM. ** $P<0.005$, *** $P<0.001$.

Supplemental Figure 5

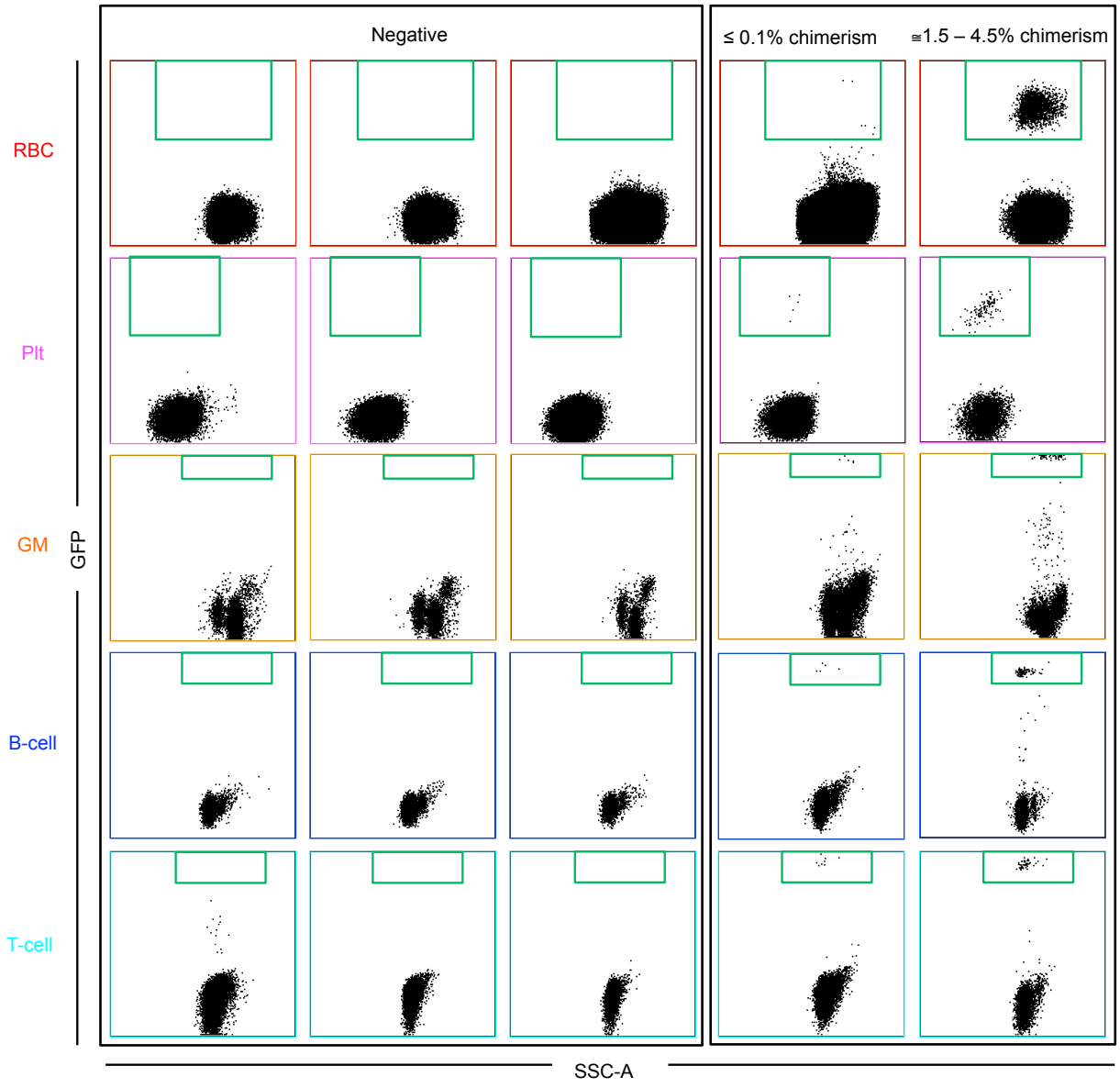

Supplemental Figure 5: Single-cell reconstitution of RBCs, Plts, GM, B, and T cells. Shown are example flow cytometry plots from single-cell transplantation experiments of one UBC-GFP cell into a lethally irradiated wt recipient. The first 3 columns show recipient mice scored as "negative", with no GFP+ cells detected, with RBCs in the top row followed by Plts, GMs, B, and T cells, as indicated. The 4th column show plots from one of the lowest "positive" recipients of each mature cell type, and the 5th (right) column) shows one plot from a robustly reconstituted recipient of each mature cell type. The level of GFP in donor-derived cells of each mature cell type matches that of the level of GFP in unmanipulated donor mice shown in Figure S1C. The use of UBC-GFP donor cells allow for very sensitive detection of donor-derived cells because the GFP signal is very distinct from wt host cells and never detected in untransplanted mice. RBC, red blood cell; Plt, platelet; GM, granulocyte-myelomonocyte.

Supplemental Figure 6

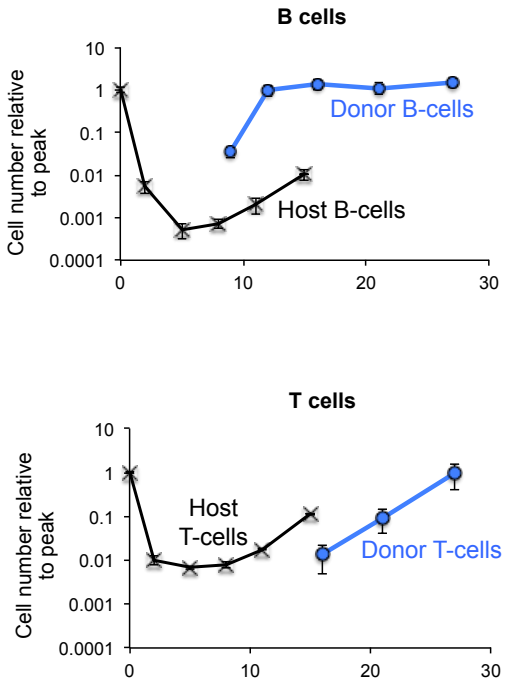

Supplemental Figure 6: CLP^{F}-derived B cells accumulate near the low point of host B cell decline, whereas host T cells recover prior to CLP-derived T cell accumulation. Black lines depict the decline and recovery of host B cells (top) and T cells (bottom) after lethal irradiation. Blue lines indicate donor-derived B cells (top) and T cells (bottom) after transplantation of CLP^{F}.

SUPPLEMENTAL METHODS

Transplantation assays

Hematopoietic cells were isolated from BM isolated from murine femurs and tibias from wild-type (C57Bl6) or UBC-GFP mice (Schaefer et al., 2001) (The Jackson Laboratory, Stock # 004353) in accordance with UCSC guidelines, as described in the supplemental methods and previously (Beaudin et al., 2014, 2016, Smith-Berdan et al., 2011, 2015; Ugarte et al., 2015). Both male and female mice were used as donors and recipients. CD117-enriched bone marrow cells were double-sorted using a FACSAriaIII (BD Biosciences) then transplanted into sublethally (~500 rads) or lethally (~1000 rads) recipients. HSC (Lineage-, cKit+, Sca1+, CD150+, FLK2-), MPP^F (Lineage-, cKit+, Sca1+, CD150-, FLK2+), CMP^- (Lineage-, $cKit^+$, $Sca1^-$, $FcγRα^{mid}$, $CD34^{mid}$, $FLK2^-$), CMP^+ (Lineage-, $cKit^+$, $Sca1^-$, $FcγRα^{mid}$, $CD34^{mid}$, $FLK2^+$), MEP (Lineage-, $cKit^+$, $Sca1^-$, $FcγRα^{lo}$, $CD34^{lo}$), classical GMP (Lineage-, $cKit^+$, $Sca1^-$, $FcγRα^{hi}$, $CD34^{hi}$), CLP (Lineage-, $cKit^{mid}$, $Sca1^{mid}$, $IL7Rα^+$, $FLK2^+$), alternative “GMPs” (Lineage-, cKit+, Sca1-, CD41-, FcγRα+), pre-GMs (Lineage-, cKit+, Sca1-, CD41-, FcγRα-, CD105-, CD150-). The lineage cocktail was comprised of CD3 (Biolegend cat #100306), CD4 (Biolegend cat #100423), CD5 (Biolegend cat #100612), CD8 (Biolegend cat #100723), TER-119 (Biolegend cat #116215), Mac1 (Biolegend cat #101217), Gr1 (Biolegend cat #108417), and B220 (Biolegend cat #103225). Antibodies used in sorting were: cKit(Biolegend cat #105826), Sca1 (Biolegend cat #122520), CD150 (Biolegend cat #115914), FLK2 (ebiosciences cat #12-1351-83), CD34 (ebiosciences cat #13-0341-85), IL7Rα (Biolegend cat #135014), CD41 (Biolegend cat #133914), CD105 (Biolegend cat #120402).

Mature cell quantification

A known volume of peripheral blood was mixed with an antibody solution [TER-119 (Biolegend cat #116210), CD61 (Biolegend cat #104314), Mac1 (Biolegend cat #101216), Gr1 (Biolegend cat #108430), B220 (Biolegend cat #103224), CD3 (Biolegend cat #100308)] containing a

known quantity of Calibrite-APC beads (BD Biosciences cat no. 340487) prior to flow cytometry analysis. For tissues, a known quantity of Calibrite-APC beads was added to each tissue preparation prior to antibody staining and analysis. The number of beads counted by flow cytometry for blood and tissue samples was used to calculate the number of mature cells per microliter of blood or within each tissue. RBC (FSC^{lo-mid}, TER-119+, CD61-, Mac1-, Gr1-, B220-, CD3-), Platelets (SSC^{lo}, TER-119-, CD61+, Mac1-, Gr1-, B220-, CD3-), GM (FSC^{mid-hi}, TER-119-, CD61-, Mac1+, Gr1+, B220-, CD3-), B-cell (FSC^{mid}, TER-119-, CD61-, Mac1-, Gr1-, B220+, CD3-), T-cell (FSC^{mid}, TER-119-, CD61-, Mac1-, Gr1-, B220-, CD3+). The distribution of mature hematopoietic cells in a mouse was measured in the blood obtained by perfusion; in bone marrow by analysis of two femurs and tibias; spleen; thymus; and lymph nodes (inguinal, axillary, and superficial cervical).

Single-cell transplants

Individual HSCs and MPP^F were double-sorted into separate wells on Terasaki plates using a FACSAriaIII from lineage-depleted bone marrow cells from UBC-GFP mice, similar to our previous reports (Byrne et al., 2017; Cole et al., 2018). Fluorescence microscopy was used to verify that only one cell occupied each well. Individual cells were loaded into a 0.5 mL syringe pre-loaded with 200,000 WT BM cells. One syringe was used per lethally irradiated (1,000 rads) WT recipient to inject one single HSC or one single MPP^F retroorbitally per recipient. Donor contribution to mature cells was assessed in the peripheral blood weekly from week 2-6 posttransplantation and every other week at later timepoints, as indicated in the x-axis of Figure 4G-J. To ensure high sensitivity, a large number of events (~2.5M) were recorded in low-engrafting recipients. The number of detected donor-derived cells was used to score a recipient as “positive”, rather than an arbitrary chimerism threshold as these percentages are highly influenced by the differential death of host cells (Figure 4O).

CFU-S analysis

Lethally irradiated (1,000 rads) WT mice were transplanted with an equal mixture of double-sorted cells isolated from mT/mG (Muzumdar et al., 2007) and UBC-GFP mice. On day 8.5 (MEP), 9.5 (CMP and CMP^F), 11.5 (MPP^F), and 13.5 (HSC) post-transplantation, mice were sacrificed and perfused to remove peripheral blood. Individual CFU-S were removed with a scalpel under a fluorescent dissecting scope. Single-cell suspensions of dissected colonies were labeled with the following antibodies: TER-119, CD41, Mac1, Gr1, and B220. Cell types were defined as follows: Erythroid Progenitor (EP; FSC^{mid-hi}, TER-119+, CD41-, Mac1-, Gr1-, B220-); Megakaryocyte (Meg; FSC^{mid-hi}, TER-119-, CD41+, Mac1-, Gr1-, B220-); GM (FSC^{mid-hi}, TER-119-, CD41-, Mac1+, Gr1+, B220-); B-cell (FSC^{mid-h},TER-119-, CD41-, Mac1-, Gr1-, B220+).

Analysis and secondary transplantation of HSC- and MPP^F-derived progenitor cells

2.5K HSC or 20K MPP^F were FACS purified from UBC-GFP mice (Schaefer et al., 2001) and transplanted into irradiated WT recipients (C57BL6) (see experimental schematic in Figure 3A) (Beaudin et al., 2014, 2016, Smith-Berdan et al., 2011, 2015; Ugarte et al., 2015). BM was isolated on days 2, 4, 7, 11 and 14 post transplantation and analyzed using the indicated markers. Neither HSCs nor MPP^Fs gave rise to FLK2+ cells due to rapid, irradiation-induced downregulation of FLK2 surface protein on both donor and host cells (manuscript in preparation); thus we utilized CD48 instead of FLK2 to assess presence of substantially overlapping “MPPs” (Figure S4A; Pietras et al., 2015). For functional analysis by secondary transplantation, BM was isolated from sternum, hips, femurs and tibias 14 days post transplantation of 2.5K HSC or 20K MPP^F, CD117-enriched, and sorted for GFP+ CMP, GMP, MEP and EP using a FACSAriaIII and the markers as displayed in Fig 3D and F. Donor-derived (GFP+) CMPs (10k cells/mouse), GMPs (50k), MEPs (50k), or EPs (20k) were then transplanted into ¾-lethally irradiated (750 rads) WT recipients (C57BL6) and mature cells from

these secondary transplants were quantified by tail bleeds and flow cytometry analysis as described in the main methods.

Host cell disappearance versus donor-derived cell production

The relative numbers and coincidence of host cell death and donor-derived cell production (Figures 4P-T and S6) were illustrated by plotting the decline in host cell numbers from pre-conditioning, set at **1**, to 30 days post-conditioning, based on data from Figure 1O. Likewise, HSC- or MPP^F-derived donor cells were set to **1** for the peak of cell production based on data from the transplantation experiments of Figure 1-2, with mature cell numbers at other time points within the 30-day period plotted relative to this peak value.

Markov Modeling

To determine if the cells observed in the quantitative plots are a result of generation of new cells or retention of generated cells, over time, we used the Markov Birth-Death Process (Kendall, 1948; Yule, 1925). Experimentally obtained population size, 7 or 9 days post-transplantation, was used as the initial population size for the modeling. Using literature derived half-lives ($T_{1/2}$) for RBCs, Plts, GM, B and T cells as 22, 4.5, 1, 38.5 and 150 days, respectively (Dholakia et al., 2015; Fulcher and Basten, 1997; Nayak et al., 2013; Simon and Kim, 2010; Sprent and Basten, 1973), we determined the death rate probability for each mature cell using the formula:

$$P(D) = \mathrm{Log}_e(2) / T_{1/2}$$

Because the population size varies differentially over time, we modified the Markov model to reflect these changes and wrote a Python code to obtain the varying birth rates, and the number of new cells produced between any two time points as depicted in Supplemental Figure 2 (dotted lines) and Supplemental Figure 3C. We also confirmed that the theoretical population size obtained based on the varying birth rates generated by the program was reflective of the experimental data at the earlier time points, where we measured the cells at “day of peak” (Figure 2A; “burst phase method”).

Python program

The complete code for the Markov birth-death models will be posted on GitHub and freely available to the scientific community upon publication of these results.

Statistical Analysis

Statistical significance was determined by two-tailed unpaired student's T-test, unless otherwise noted. All data are shown as mean ± standard error of the mean (SEM) representing at least two independent experiments.

SUPPLEMENTAL REFERENCES

Beaudin, A.E., Boyer, S.W., and Forsberg, E.C. (2014). Flk2/Flt3 promotes both myeloid and lymphoid development by expanding non-self-renewing multipotent hematopoietic progenitor cells. Exp. Hematol. *42*, 218–229.e4.

Beaudin, A.E., Boyer, S.W., Perez-Cunningham, J., Hernandez, G.E., Derderian, S.C., Jujjavarapu, C., Aaserude, E., MacKenzie, T., and Forsberg, E.C. (2016). A Transient Developmental Hematopoietic Stem Cell Gives Rise to Innate-like B and T Cells. Cell Stem Cell *19*, 768–783.

Dholakia, U., Bandyopadhyay, S., Hod, E.A., and Prestia, K.A. (2015). Determination of RBC survival in C57BL/6 and C57BL/6-Tg(UBC-GFP) mice. Comp. Med.754-61.

Fulcher, D., and Basten, A. (1997). B cell life span: a review. Immunol. Cell Biol.

Kendall, D.G. (1948). On the Generalized “Birth-and-Death” Process. Ann. Math. Stat.

Muzumdar, M.D., Tasic, B., Miyamichi, K., Li, L., and Luo, L. (2007). A global double-fluorescent Cre reporter mouse. Genesis *45*, 593–605.

Nayak, M.K., Kulkarni, P.P., and Dash, D. (2013). Regulatory role of proteasome in determination of platelet life span. J. Biol. Chem. 288(10):6826-34.

Pietras EM, Reynaud D, Kang YA, Carlin D, Calero-Nieto FJ, Leavitt AD, Stuart JM, Göttgens B, Passegué E. (2015). Functionally Distinct Subsets of Lineage-Biased Multipotent Progenitors Control Blood Production in Normal and Regenerative Conditions. Cell Stem Cell.17(1):35-46.

Schaefer, B.C., Schaefer, M.L., Kappler, J.W., Marrack, P., and Kedl, R.M. (2001). Observation of Antigen-Dependent CD8+ T-Cell/ Dendritic Cell Interactions in Vivo. Cell. Immunol. *214*, 110–122.

Simon, S.I., and Kim, M.H. (2010). A day (or 5) in a neutrophil’s life. Blood.

Smith-Berdan, S., Nguyen, A., Hassanein, D., Zimmer, M., Ugarte, F., Ciriza, J., Li, D., García-Ojeda, M.E., Hinck, L., and Forsberg, E.C. (2011). Robo4 cooperates with CXCR4 to specify hematopoietic stem cell localization to bone marrow niches. Cell Stem Cell *8*, 72–83.

Smith-Berdan, S., Nguyen, A., Hong, M.A., and Forsberg, E.C. (2015). ROBO4-mediated vascular integrity regulates the directionality of hematopoietic stem cell trafficking. Stem Cell Reports *4*, 255–268.

Sprent, J., and Basten, A. (1973). Circulating T and B lymphocytes of the mouse. II. Lifespan. Cell. Immunol.

Ugarte, F., Sousae, R., Cinquin, B., Martin, E.W., Krietsch, J., Sanchez, G., Inman, M., Tsang, H., Warr, M., Passegué, E., et al. (2015). Progressive Chromatin Condensation and H3K9 Methylation Regulate the Differentiation of Embryonic and Hematopoietic Stem Cells. Stem Cell Reports *5*, 728–740.

Yule, G.U. (1925). A Mathematical Theory of Evolution, Based on the Conclusions of Dr. J. C.